

From Free-Energy Profiles to Activation Free Energies

Johannes C. B. Dietschreit,¹ Dennis J. Diestler,² Andreas Hulm,³ Christian Ochsenfeld,^{3,4} and Rafael Gómez-Bombarelli^{1, a)}

¹⁾ *Department of Materials Science and Engineering, Massachusetts Institute of Technology, Cambridge, Massachusetts 02139, USA*

²⁾ *University of Nebraska-Lincoln, Lincoln, Nebraska 68583, USA*

³⁾ *Chair of Theoretical Chemistry, Department of Chemistry, University of Munich (LMU), Butenandtstr. 7, D-81377 München, Germany*

⁴⁾ *Max Planck Institute for Solid State Research, Heisenbergstr. 1, D-70569 Stuttgart, Germany*

(Dated: 20.4.2023)

Given a chemical reaction going from reactant (R) to the product (P) on a potential energy surface (PES) and a collective variable (CV) discriminating between R and P, we define the free-energy profile (FEP) as the logarithm of the marginal Boltzmann distribution of the CV. This FEP is not a true free energy. Nevertheless, it is common to treat the FEP as the “free-energy” analog of the minimum potential energy path and to take the activation free energy, $\Delta F_{\text{RP}}^\ddagger$, as the difference between the maximum at the transition state and the minimum at R. We show that this approximation can result in large errors. The FEP depends on the CV and is therefore not unique. For the same reaction different, discriminating CVs can yield different $\Delta F_{\text{RP}}^\ddagger$. We derive an exact expression for the activation free energy that avoids this ambiguity. We find $\Delta F_{\text{RP}}^\ddagger$ to be a combination of the probability of the system being in the reactant state, the probability density on the dividing surface, and the thermal de Broglie wavelength associated with the transition. We apply our formalism to simple analytic models and realistic chemical systems and show that the FEP-based approximation applies only at low temperatures for CVs with a small effective mass. Most chemical reactions occur on complex, high-dimensional PES that cannot be treated analytically and pose the added challenge of choosing a good CV. We study the influence of that choice and find that, while the reaction free energy is largely unaffected, $\Delta F_{\text{RP}}^\ddagger$ is quite sensitive.

I. INTRODUCTION

Computer simulations of chemical systems are valuable for the explanation of their experimental counterparts. In the case of chemical reactions, quantities of primary interest are equilibrium constants and reaction rate constants, or quantities directly related to these, i.e., the reaction free energy ΔF_{RP} (difference between free energies of products and reactants) and the activation free energy $\Delta F_{\text{RP}}^\ddagger$ (the difference between free energies of transition state and reactants). Indeed, the computation of such free energy differences has a long history.^{1–7}

The kinetics of a chemical reaction can be modeled as a transition from a reactant well (R) on the potential energy surface (PES) to a product well (P). The two local minima are separated by a potential energy barrier that must be overcome as the atomic configuration changes and the reaction progresses. The total configuration space is partitioned into (hyper) volumes corresponding to R and P by a dividing (hyper) surface, the separatrix. The atomic rearrangement is described by a collective variable (CV) (or reaction coordinate), which is a function of some subset of Cartesian coordinates that gives the degree of reaction progress (e.g., 0 at R and 1 at P). In order to describe a reaction well, one needs to

choose a “good” CV, i.e., one that distinguishes properly between configurations of R and P. The CV is chosen so that it has two non-overlapping domains that correspond to the domains of R and P. It is practically impossible to find the optimal CV for a complex realistic system.⁸ One must therefore base the choice of CV either on chemical intuition or on recently developed machine learning-based methods.^{9–13}

The free-energy profile (FEP)¹⁴ (also referred to as the potential of mean force) is defined, up to a scaling constant, as the logarithm of the marginal Boltzmann distribution of the CV (Fig. 1). The FEP is determined in practice by molecular dynamics (MD) or Monte Carlo simulations. Because R and P are often separated by high potential energy barriers that are not overcome on simulation timescales, special simulation techniques, such as importance-sampling algorithms, must often be employed to sample configuration space properly.^{15–22} These algorithms usually directly yield the FEP.

Contrary to what the name implies, the FEP is not a true Helmholtz or Gibbs free energy.²³ Treating the FEP as if it were a free-energy analog of the minimum energy path is pervasive in the field and rarely acknowledged explicitly as the approximation that it is. Differences in the FEP between local extrema are then misinterpreted as reaction and activation free energies (see red highlight in Fig. 1). We have recently shown that this misconception leads to significant errors in reaction free energies, ΔF_{RP} .²³ The choice of the CV has a large influence on

^{a)} Electronic mail: rafagb@mit.edu

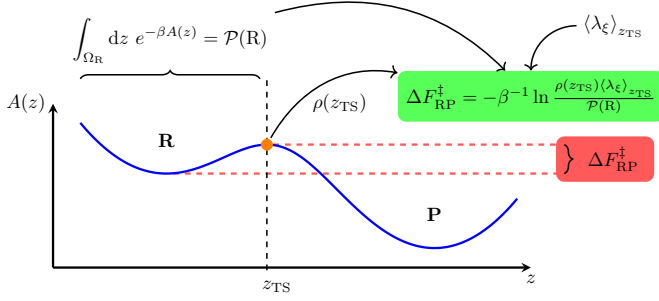


FIG. 1. Schematic summary of the present work showing an FEP with minima corresponding to reactant (R) and product (P) separated by a maximum. Commonly assumed, but incorrect, expression for activation free energy highlighted in red. The expression derived in this work is highlighted in green.

the FEP. In fact, the FEP has no meaning independent of the CV^{23–25} and the structure of the FEP (e.g., the breadth and depth of local extrema or even their existence) depends on the CV. Thus, a treatment that relies solely on the shape of the FEP yields CV-dependent activation free energies. Moreover, kinetic quantities (e.g., ΔF_{RP}^\ddagger) derived from the FEP, which depends solely on the PES and does not account for particle masses, must be approximations. The rigorous formula for ΔF_{RP}^\ddagger derived here (see green highlight of Fig. 1 and Sec. II E) is independent of the precise mathematical form of the CV, as long as it discriminates between R and P. We show below that a poor choice of CV has an even bigger impact on ΔF_{RP}^\ddagger than on ΔF_{RP} .

The remainder of the article is organized as follows. In Section II we first derive an expression for the rate constant $k_{R \rightarrow P}$. Then, using the Eyring equation, we derive the connection between ΔF_{RP}^\ddagger and $k_{R \rightarrow P}$. The physical interpretation of the components that constitute the correct activation free energy is discussed. In Section III we employ simple analytic models to assess the error incurred by the common practice of taking ΔF_{RP}^\ddagger to be the difference between the values of the FEP at the maximum (transition state) and the minimum at R. Section IV is devoted to an analysis of the sensitivity of ΔF_{RP} and ΔF_{RP}^\ddagger to the choice of the CV. To emphasize the errors that can result from estimating ΔF_{RP}^\ddagger directly from the FEP, we examine in Section V a numerical one-dimensional model and two realistic chemical processes. Section VI consists of a summary of our findings and a discussion of open questions on the computation of the activation free energy. Our conclusions are summarized in Section VII.

II. THEORY

A. Description of the System

The interconversion of R and P is represented by the chemical reaction



State $\alpha (=R, P)$ is defined by the region of configuration space it occupies, designated by Ω_α . Thus, we define the configuration integral associated with the state α by

$$Z_\alpha = \int_{\Omega_\alpha} d\mathbf{x} e^{-\beta U(\mathbf{x})}. \quad (2)$$

Here $\mathbf{x} = (x_1, x_2, \dots, x_{3N})^T$ denotes the column vector of Cartesian coordinates that specify the atomic configuration; $d\mathbf{x} = \prod_{i=1}^{3N} dx_i$ is the $3N$ -dimensional volume element; $U(\mathbf{x})$ is the potential energy surface (PES), and $\beta \equiv 1/k_B T$. Only those configurations \mathbf{x} that belong to Ω_α contribute to Z_α , which is the effective volume of configuration space occupied by state α . We assume that Ω_R and Ω_P constitute the whole configuration space available to the system and they are separated by a $(3N-1)$ -dimensional dividing (hyper) surface, normally taken to contain the ridge of the barrier of the PES between the minima corresponding to R and P.

The course of the reaction can be monitored by a (scalar) CV (or reaction coordinate), $\xi(\mathbf{x})$, which is a function of a subset of the atomic coordinates that gives a measure of the progress of the reaction. The CV is chosen such that Ω_R and Ω_P correspond to non-overlapping domains of the CV. Ideally the gradient of $\xi(\mathbf{x})$ should be normal to the dividing surface, on which the CV assumes a particular value z_{TS} . In this case the CV discriminates properly between R and P.

It is convenient to introduce mass-weighted coordinates

$$\tilde{\mathbf{x}} = \mathbf{M}^{1/2} \mathbf{x}, \quad (3)$$

where \mathbf{M} stands for the $3N \times 3N$ diagonal matrix of atomic masses. In terms of mass-weighted coordinates the Hamiltonian is

$$\begin{aligned} \mathcal{H} &= \frac{1}{2} \sum_{i=1}^{3N} \tilde{p}_i^2 + U(\tilde{x}_1, \tilde{x}_2, \dots, \tilde{x}_{3N}) \\ &= \frac{1}{2} \tilde{\mathbf{p}}^T \tilde{\mathbf{p}} + U(\tilde{\mathbf{x}}), \end{aligned} \quad (4)$$

where $\tilde{p}_i = \dot{\tilde{x}}_i$ is the momentum conjugate to the coordinate \tilde{x}_i . Henceforth we employ the condensed notation of the second line of eq. (4), where $\tilde{\mathbf{p}}$ stands for the column vector of momenta.

B. Curvilinear Coordinates

The treatment of the reaction rate is facilitated by employment of a special set of coordinates, one of which

is the CV. Hence, we transform from mass-weighted coordinates to a complete set of curvilinear coordinates, $\mathbf{q} = \mathbf{q}(\tilde{\mathbf{x}})$, of which we take $q_1(\tilde{\mathbf{x}}) = \xi(\tilde{\mathbf{x}})$. From the inverse transformation $\tilde{\mathbf{x}} = \tilde{\mathbf{x}}(\mathbf{q})$ we obtain

$$\dot{\tilde{\mathbf{x}}} = \mathbf{J}\dot{\mathbf{q}}, \quad (5)$$

where $[\mathbf{J}]_{ij} = \frac{\partial \tilde{x}_i}{\partial q_j}$ is an element of the Jacobian. The momentum conjugate to \mathbf{q} is

$$\mathbf{p} = \mathbf{M}_q \dot{\mathbf{q}}, \quad (6)$$

where

$$\mathbf{M}_q = \mathbf{J}^T \mathbf{J}, \quad (7)$$

the mass matrix in curvilinear coordinates, is also referred to as the mass-metric tensor (see, for example, Refs. 2,26–28). In general, \mathbf{M}_q is a full matrix. The Hamiltonian is given in curvilinear coordinates by

$$\mathcal{H} = \frac{1}{2} \mathbf{p}^T \mathbf{M}_q^{-1} \mathbf{p} + U(\mathbf{q}). \quad (8)$$

From eq. (7) we deduce the following expression for the effective inverse mass matrix

$$\begin{aligned} [\mathbf{M}_q^{-1}]_{ij} &= \sum_{k=1}^{3N} [\mathbf{J}^{-1}]_{ik} [\mathbf{J}^{-1}]_{kj} \\ &= (\nabla_{\tilde{\mathbf{x}}} q_i)^T (\nabla_{\tilde{\mathbf{x}}} q_j), \end{aligned} \quad (9)$$

where we employ $[\mathbf{J}^{-1}]_{ik} = \frac{\partial q_i}{\partial \tilde{x}_k}$ and $(\nabla_{\tilde{\mathbf{x}}} q_i)^T = (\partial q_i / \partial \tilde{x}_1, \partial q_i / \partial \tilde{x}_2, \dots, \partial q_i / \partial \tilde{x}_{3N})$ is the $3N$ -dimensional mass-weighted gradient. Using eq. (3), we get from eq. (9)

$$[\mathbf{M}_q^{-1}]_{ij} = (\nabla_{\mathbf{x}} q_i)^T \mathbf{M}^{-1} (\nabla_{\mathbf{x}} q_j) \quad (10)$$

Note the distinction between $\nabla_{\mathbf{x}}$ for the Cartesian gradient and $\nabla_{\tilde{\mathbf{x}}}$ for the gradient with respect to mass-weighted coordinates.

C. Reaction Rate Constant

We assume the system to be in thermodynamic equilibrium. Then the rate of the forward reaction equals the rate of the backward reaction

$$k_{R \rightarrow P} \mathcal{P}(R) = k_{P \rightarrow R} \mathcal{P}(P), \quad (11)$$

where $k_{R \rightarrow P}$ and $k_{P \rightarrow R}$ are the forward and backward rate constants, and $\mathcal{P}(R)$ and $\mathcal{P}(P)$ are the respective probabilities of observing R and P. The rate can also be

expressed in terms of the frequency ν of crossing the dividing surface in either the forward or backward direction (i.e., of the number of times per unit time that $\xi(\tilde{\mathbf{x}}) - z_{\text{TS}}$ changes sign). Since the forward and backward rates are equal, then either rate must equal $\nu/2$. Thus, focusing on the forward rate, we have from eq. (11)

$$k_{R \rightarrow P} = \frac{\nu}{2\mathcal{P}(R)} \quad (12)$$

The following alternative expression for the rate constant is frequently used:^{29–34}

$$k_{R \rightarrow P} = \frac{\langle \dot{\xi} \Theta(\dot{\xi}) \delta(\xi(\tilde{\mathbf{x}}) - z_{\text{TS}}) \rangle_{p,q}}{\langle \Theta(z_{\text{TS}} - \xi(\tilde{\mathbf{x}})) \rangle_{p,q}} \quad (13)$$

Here $\langle \rangle_{p,q}$ denotes the ensemble average over all of phase space, δ the Dirac delta function, Θ the Heaviside function, and $\dot{\xi}$ the time derivative of the CV. The equivalency of the two expressions is proven in the supplementary material.

D. Frequency of Crossing the Dividing Surface

The frequency of crossing the dividing surface can be expressed formally as the time average of the frequency with which $\xi(\tilde{\mathbf{x}}) - z_{\text{TS}}$ changes sign³⁵:

$$\begin{aligned} \nu &= \lim_{\tau \rightarrow \infty} \frac{1}{\tau} \int_0^\tau dt \left| \frac{d}{dt} \Theta[\xi(\tilde{\mathbf{x}}(t)) - z_{\text{TS}}] \right| \\ &= \lim_{\tau \rightarrow \infty} \frac{1}{\tau} \int_0^\tau dt \left| (\dot{\tilde{\mathbf{x}}}(t))^T \nabla_{\tilde{\mathbf{x}}} \xi(\tilde{\mathbf{x}}(t)) \right| \delta(\xi(\tilde{\mathbf{x}}(t)) - z_{\text{TS}}) \end{aligned} \quad (14)$$

A proof of this expression is provided in the supplementary material. Assuming the system to be ergodic, we can recast the time average as an ensemble average

$$\nu = \frac{\int d\tilde{\mathbf{x}} \int d\tilde{\mathbf{p}} e^{-\beta \mathcal{H}} \left| \dot{\tilde{\mathbf{x}}}^T \nabla_{\tilde{\mathbf{x}}} \xi(\tilde{\mathbf{x}}) \right| \delta(\xi(\tilde{\mathbf{x}}) - z_{\text{TS}})}{\int d\tilde{\mathbf{x}} \int d\tilde{\mathbf{p}} e^{-\beta \mathcal{H}}}, \quad (15)$$

where \mathcal{H} is given by eq. (4). We next transform from mass-weighted to curvilinear coordinates. From eqs. (5), (6), and (7) we get

$$\dot{\tilde{\mathbf{x}}}^T \nabla_{\tilde{\mathbf{x}}} \xi = \mathbf{p}^T \mathbf{J}^{-1} \nabla_{\tilde{\mathbf{x}}} \xi = \sum_{i=1}^{3N} p_i (\nabla_{\tilde{\mathbf{x}}} q_i)^T \nabla_{\tilde{\mathbf{x}}} \xi, \quad (16)$$

where the second equality invokes the definition of the inverse Jacobian. Substitution of eq. (16) into eq. (15) and transformation to curvilinear coordinates yields

$$\nu = \frac{\int d\mathbf{q} e^{-\beta U(\mathbf{q})} \int d\mathbf{p} e^{-\frac{\beta}{2} \mathbf{p}^T \mathbf{M}_q^{-1} \mathbf{p}} \left| \sum_{i=1}^{3N} p_i (\nabla_{\bar{\mathbf{x}}} q_i)^T \nabla_{\bar{\mathbf{x}}} \xi \right| \delta(\xi(\mathbf{q}) - z_{\text{TS}})}{\int d\mathbf{q} e^{-\beta U(\mathbf{q})} \int d\mathbf{p} e^{-\frac{\beta}{2} \mathbf{p}^T \mathbf{M}_q^{-1} \mathbf{p}}} \quad (17)$$

To simplify this expression we exploit the freedom afforded by curvilinear coordinates. While the “first” is chosen to be the CV, the remaining $3N - 1$ are as yet unspecified. Hence, we require that q_2, q_3, \dots, q_{3N} be *orthogonal* to $q_1 = \xi$, which constraint is expressed by

$$(\nabla_{\bar{\mathbf{x}}} q_i)^T \nabla_{\bar{\mathbf{x}}} \xi = 0, \quad i = 2, 3, \dots, 3N \quad (18)$$

In general, the construction of the orthogonal set can be achieved in a variety of ways.¹⁶

Invoking eq. (18), we can express the kinetic energy as

$$\begin{aligned} \frac{1}{2} \mathbf{p}^T \mathbf{M}_q^{-1} \mathbf{p} &= \frac{1}{2} \sum_{i=1}^{3N} \sum_{j=1}^{3N} p_i (\nabla_{\bar{\mathbf{x}}} q_i)^T (\nabla_{\bar{\mathbf{x}}} q_j) p_j \\ &= \frac{1}{2} |\nabla_{\bar{\mathbf{x}}} \xi|^2 p_1^2 + \sum_{i=2}^{3N} \sum_{j=2}^{3N} p_i (\nabla_{\bar{\mathbf{x}}} q_i)^T (\nabla_{\bar{\mathbf{x}}} q_j) p_j \\ &= \frac{1}{2} |\nabla_{\bar{\mathbf{x}}} \xi|^2 p_1^2 + \frac{1}{2} \mathbf{p}'^T \mathbf{M}'^{-1} \mathbf{p}' \end{aligned} \quad (19)$$

where in analogy to eq. (9) we define the $(3N - 1) \times (3N - 1)$ inverse mass matrix \mathbf{M}'^{-1} and the $(3N - 1)$ -dimensional momentum vector $\mathbf{p}' = (p_2, p_3, \dots, p_{3N})^T$. Likewise, we can simplify eq. (16)

$$\sum_{i=1}^{3N} p_i (\nabla_{\bar{\mathbf{x}}} q_i)^T \nabla_{\bar{\mathbf{x}}} \xi = |\nabla_{\bar{\mathbf{x}}} \xi|^2 p_1 \quad (20)$$

Plugging eqs. (19) and (20) into eq. (17), we get

$$\nu = \frac{\int d\mathbf{q} e^{-\beta U(\mathbf{q})} \delta(\xi(\mathbf{q}) - z_{\text{TS}}) \left(\int_{-\infty}^{\infty} dp_1 |p_1| e^{-\frac{\beta |\nabla_{\bar{\mathbf{x}}} \xi|^2 p_1^2}{2}} |\nabla_{\bar{\mathbf{x}}} \xi|^2 \right) \int d\mathbf{p}' e^{-\frac{\beta}{2} \mathbf{p}'^T \mathbf{M}'^{-1} \mathbf{p}'}}{\int d\mathbf{q} e^{-\beta U(\mathbf{q})} \int d\mathbf{p} e^{-\frac{\beta}{2} \mathbf{p}^T \mathbf{M}_q^{-1} \mathbf{p}}} \quad (21)$$

Performing the integration on p_1 gives

$$\nu = 2k_B T \frac{\int d\mathbf{q} e^{-\beta U(\mathbf{q})} \delta(\xi(\mathbf{q}) - z_{\text{TS}}) \cdot 1 \cdot \int d\mathbf{p}' e^{-\frac{\beta}{2} \mathbf{p}'^T \mathbf{M}'^{-1} \mathbf{p}'}}{\int d\mathbf{q} e^{-\beta U(\mathbf{q})} \int d\mathbf{p} e^{-\frac{\beta}{2} \mathbf{p}^T \mathbf{M}_q^{-1} \mathbf{p}}} \quad (22)$$

Inserting the identity $1 = |\nabla_{\bar{\mathbf{x}}} \xi| (2\pi k_B T)^{-1/2} \int_{-\infty}^{\infty} dp_1 e^{-\frac{\beta |\nabla_{\bar{\mathbf{x}}} \xi|^2 p_1^2}{2}}$ into eq. (22) at the place indicated, we obtain

$$\nu = \sqrt{\frac{2k_B T}{\pi}} \frac{\int d\mathbf{q} e^{-\beta U(\mathbf{q})} \int d\mathbf{p} e^{-\frac{\beta}{2} \mathbf{p}^T \mathbf{M}_q^{-1} \mathbf{p}} |\nabla_{\bar{\mathbf{x}}} \xi| \delta(\xi(\mathbf{q}) - z_{\text{TS}})}{\int d\mathbf{q} e^{-\beta U(\mathbf{q})} \int d\mathbf{p} e^{-\frac{\beta}{2} \mathbf{p}^T \mathbf{M}_q^{-1} \mathbf{p}}} \quad (23)$$

Transforming back to Cartesian coordinates yields

$$\nu = \sqrt{\frac{2k_B T}{\pi}} \langle \delta(\xi(\mathbf{x}) - z_{\text{TS}}) |\nabla_{\bar{\mathbf{x}}} \xi| \rangle, \quad (24)$$

where $\langle \rangle$ indicates the ensemble average over configuration space. Using the fact that

$$\rho(z) = \langle \delta(\xi(\mathbf{x}) - z) \rangle = Z^{-1} \int d\mathbf{x} \delta(\xi(\mathbf{x}) - z) e^{-\beta U(\mathbf{x})} \quad (25)$$

is the normalized probability density of observing an atomic configuration \mathbf{x} such that $\xi(\mathbf{x}) = z$, we can re-

cast eq. (24) as

$$\begin{aligned} \nu &= \sqrt{\frac{2k_B T}{\pi}} \rho(z_{\text{TS}}) \langle |\nabla_{\bar{\mathbf{x}}} \xi| \rangle_{z_{\text{TS}}} \\ &= \sqrt{\frac{2k_B T}{\pi}} \rho(z_{\text{TS}}) \left\langle \sqrt{(\nabla_{\mathbf{x}} \xi)^T \mathbf{M}^{-1} (\nabla_{\mathbf{x}} \xi)} \right\rangle_{z_{\text{TS}}} \\ &= \left\langle \sqrt{\frac{2k_B T}{\pi m_\xi}} \right\rangle_{z_{\text{TS}}} \rho(z_{\text{TS}}), \end{aligned} \quad (26)$$

where $\langle \rangle_{z_{\text{TS}}}$ signifies an average over the dividing surface. The second line of eq. (26) follows from eq. (3); the

third line implicitly defines m_ξ , which we interpret as the effective mass of the pseudo-particle associated with the coordinate $\xi(\mathbf{x})$:

$$m_\xi^{-1} = (\nabla_{\mathbf{x}}\xi)^T \mathbf{M}^{-1} (\nabla_{\mathbf{x}}\xi) = [\mathbf{M}_q^{-1}]_{11} , \quad (27)$$

which is the 1,1 element of the inverse mass-metric tensor (see eq. (10)).^{2,26–28} Finally, combining eqs. (12) and (26), we obtain

$$k_{R \rightarrow P} = \left\langle \sqrt{\frac{k_B T}{2\pi m_\xi}} \right\rangle_{z_{TS}} \frac{\rho(z_{TS})}{\mathcal{P}(R)} . \quad (28)$$

E. Free Energy of Activation

Eyring's equation relates the rate constant to a free energy of activation by defining a modified equilibrium constant for the formation of activated complex from reactant R (see, for example, Ref 36). In the present notation the equation is

$$k_{R \rightarrow P} = \frac{k_B T}{h} e^{-\beta \Delta F_{RP}^\ddagger} , \quad (29)$$

where h is Planck's constant. We use the symbol F for the Helmholtz free energy in order to distinguish it from the free-energy profile denoted by A (see eq. (32)). We solve eq. (29) for the activation free energy and combine the result with eq. (28) to get

$$\Delta F_{RP}^\ddagger = -k_B T \ln \frac{\rho(z_{TS}) \langle \lambda_\xi \rangle_{z_{TS}}}{\mathcal{P}(R)} , \quad (30)$$

where $\lambda_\xi \equiv \sqrt{h^2/2\pi m_\xi k_B T}$. We interpret λ_ξ as the de Broglie thermal wavelength of the pseudo-particle associated with the CV.

By expanding the logarithm in eq. (30) we can recast the “exact” expression for the activation free energy as

$$\begin{aligned} \Delta F_{RP}^\ddagger &= -k_B T \ln \rho(z_{TS}) + k_B T \ln \mathcal{P}(R) - k_B T \ln \langle \lambda_\xi \rangle_{z_{TS}} \\ &= A(z_{TS}) + k_B T \ln \int_{\Omega_R} dz \rho(z) - k_B T \ln \langle \lambda_\xi \rangle_{z_{TS}} \end{aligned} \quad (31)$$

The second line of eq. (31) depends on the definition of the free-energy profile (FEP)^{16,23}

$$A(z) = -k_B T \ln \rho(z) , \quad (32)$$

and on the relation²³

$$\mathcal{P}(R) = \int_{\Omega_R} dz \rho(z) . \quad (33)$$

A frequently employed procedure is to set the activation free energy equal to the difference between the maximum of the FEP at z_{TS} and the minimum at $z_{R,\min}$:

$$\Delta \tilde{F}_{RP}^\ddagger = A(z_{TS}) - A(z_{R,\min}) \quad (34)$$

We place a tilde on this formula to distinguish it from the “exact” one in eq. (30). Thus, $\Delta \tilde{F}_{RP}^\ddagger$ can be viewed as an approximation. For example, if the density is strongly peaked about $z_{R,\min}$, then $k_B T \ln \mathcal{P}(R) \approx -A(z_{R,\min})$, according to eqs. (32) and (33). Under this condition the approximate formula agrees with the exact, except for the term $-k_B T \ln \langle \lambda_\xi \rangle_{z_{TS}}$. Therefore the influence of distortions of the coordinate system induced by $\xi(\mathbf{x})$ is ignored by $\Delta \tilde{F}_{RP}^\ddagger$, as is the influence of mass (see eq. (27)).

An alternative recasting of the exact formula for the activation free energy, eq. (30), is instructive. Invoking the relations²³

$$q_R = \frac{Z_R}{\Lambda} \quad (35)$$

and

$$\mathcal{P}(R) = \frac{Z_R}{Z} , \quad (36)$$

where q_R is the molecular partition function of R and $\Lambda \equiv \prod_{i=1}^{3N} \sqrt{h^2/2\pi m_i k_B T}$ (the product of all Cartesian de Broglie wavelengths), we rewrite the exact expression as

$$\begin{aligned} \Delta F_{RP}^\ddagger &= -k_B T \ln \left[\frac{Z \rho(z_{TS}) \langle \lambda_\xi \rangle_{z_{TS}}}{\Lambda q_R} \right] \\ &= -k_B T \ln \left[Z \rho(z_{TS}) \frac{\langle \lambda_\xi \rangle_{z_{TS}}}{\Lambda} \right] + k_B T \ln q_R \end{aligned} \quad (37)$$

The second term on the right side of eq. (37) is the (negative of the) free energy of R.²³ Likewise, if we regard $q^\ddagger \equiv Z \rho(z_{TS}) \frac{\langle \lambda_\xi \rangle_{z_{TS}}}{\Lambda}$ as the effective partition function with z fixed at z_{TS} , then the first term is the free energy of the constrained system. That q^\ddagger has the stated character can be demonstrated explicitly in case the curvilinear coordinates form a complete orthogonal set. Then we can rewrite eq. (37) as

$$\begin{aligned} \Delta F_{RP}^\ddagger &= -k_B T \ln q^\ddagger + k_B T \ln q_R \\ &= F^\ddagger - F_R \end{aligned} \quad (38)$$

This form of ΔF_{RP}^\ddagger is very intuitive: The activation free energy is the difference between the free energy of the system constrained to the dividing surface, F^\ddagger , and the free energy of the reactant, F_R . Moreover, it is noteworthy that eq. (38) assumes the same form as the corresponding expression derived by conventional transition state theory.³⁶

III. IMPACT OF APPROXIMATING THE ACTIVATION FREE ENERGY

In order to gauge the error incurred by approximating the activation free energy $\Delta \tilde{F}_{RP}^\ddagger$ (eq. (34)) in comparison to the “exact” ΔF_{RP}^\ddagger (eq. (30)) we study the behavior of two analytically treatable models. Each consists

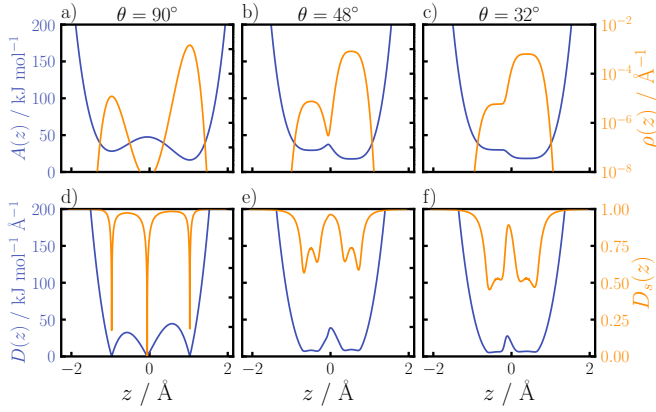


FIG. 3. Top panel, plots of probability density (right ordinate, orange curve) and FEP (left ordinate, blue curve), and bottom panel $D(z)$ (left ordinate, blue curve) and $D_s(z)$ (right ordinate, orange curve) for three choices of CV: a) $\theta = 90^\circ$, b) $\theta = 48^\circ$ (maximum in Fig. 4c), and c) $\theta = 32^\circ$, last value for which the FEP still has a detectable local maximum.

yield realistic free energies ($\Delta F_{\text{RP}} = -12.28$ kJ/mol and $\Delta F_{\text{RP}}^\ddagger = 16.06$ kJ/mol, which is roughly the activation free energy of the internal rotation of butane³⁷). The ideal CV is $\xi(x, y) = x$ and the dividing surface coincides with the line $x = x_{\text{max}} = -0.06725$ (see Fig. 2). Clearly, $\nabla \xi \cdot \nabla U$ vanishes on \mathcal{S} , which is the constraint that should be obeyed by a CV that properly discriminates between R and P.³⁵

To vary the choice of the CV systematically, we define the CV by

$$\xi(x, y) = ax + (1 - a)y \quad (44)$$

where a is restricted to the interval $[0, 1]$. We determine the value of a by specifying the angle θ between $\nabla \xi$ and $\mathbf{e}_{\mathcal{S}}$, the unit vector parallel with the true separatrix \mathcal{S} (i.e., \mathbf{e}_y). In other words, a , and therefore ξ , are determined by the condition $\frac{\nabla \xi}{|\nabla \xi|} \cdot \mathbf{e}_{\mathcal{S}} = \cos \theta$. (Details of the calculation are provided in the supplementary material.) Corresponding to a given θ (i.e., a given choice of the CV) is a “trial” separatrix $S(\theta)$, which is a line having the equation $y = -a(x - x_{\text{max}})/(1 - a)$, where x_{max} is the x -coordinate of the saddle point on the PES. When $a = 1$, then $\theta = 90^\circ$. In this limit $S(90^\circ)$ coincides with \mathcal{S} . As a decreases from 1 to 0, $S(\theta)$ rotates counterclockwise about the point $(x_{\text{max}}, 0)$. The trial separatrix $S(45^\circ)$ is shown in Fig. 2. In the limit $a = 0$, $\nabla \xi = \mathbf{e}_y$, $\theta = 0$. Hence, $S(0^\circ)$ is normal to \mathcal{S} , which makes $\xi(x, y) = y$ the worst possible choice of the CV.

For a given θ , we calculate the probability density $\rho(z)$ using eq. (25). As shown in the supplementary material, the evaluation of the required double integrals is facilitated by transforming from Cartesian to orthogonal coordinates $q_1 = \xi(x, y)$ and $q_2 = (a - 1)x + ay$. We obtain the FEP using eq. (32). Illustrative plots of $\rho(z)$ and $A(z)$ are shown in Fig. 3a-c for three CV choices. The local maximum of the FEP, z_{max} , defines the domains of R

and P. We note, however, that the FEPs for $\theta < 32^\circ$ lack any such local maximum. We henceforth ignore these choices, as the CV cannot distinguish R from P at all.

As a measure of the quality of the chosen CV, we adopt a modification of the procedure introduced previously²³, which was to monitor the quantity $D(z) = \langle |\nabla \xi(\mathbf{x}) \cdot \nabla U(\mathbf{x})| \rangle_z$. We note that $D(z_{\text{TS}})$ is exactly zero on \mathcal{S} for the ideal CV (i.e., the one that discriminates perfectly between R and P). However, away from \mathcal{S} , or in case the choice of CV is not ideal, $D(z)$ is difficult to interpret, because it depends so strongly on the local gradient of the PES. To ameliorate this defect we propose a scaled, dimensionless orthogonality measure defined by

$$D_s(z) = \left\langle \left| \frac{\nabla \xi(\mathbf{x})}{|\nabla \xi(\mathbf{x})|} \cdot \frac{\nabla U(\mathbf{x})}{|\nabla U(\mathbf{x})|} \right| \right\rangle_z, \quad (45)$$

where we replace the gradients of U and ξ with their corresponding unit vectors. Thus, $D_s(z_{\text{TS}})$ is zero on \mathcal{S} for the ideal CV, where the gradients of U and ξ are perpendicular, and unity where they are parallel.

One can see in Fig. 3d that for the ideal CV $\xi(x, y) = x$, D and D_s have very sharp roots at z_{TS} , indicating that the CV is orthogonal to the separatrix. Because of the symmetry of the PES, the two measures have two additional roots located at the minima of reactant and product. D_s does not actually reach zero on account of the finite numerical resolution of our computation. However, the sharp minima are still visible. Figures 3e and 3f show the orthogonality measure for non-ideal CVs. The shape of the D -measures changes drastically. Most significantly, the sharp root or minimum at the maximum of the FEP turns into a local maximum for both D and D_s , which is an unmistakable sign that results for these CVs cannot be trusted (see the dependence of the $\Delta F_{\text{RP}}^\ddagger$ on θ in Fig. 4).

Using the numerically computed $\rho(z)$, we calculate the reaction free energy and activation free energy, which are given, respectively, by eq. (42) and eq. (30), where we set $z_{\text{TS}} = z_{\text{max}}$. In Fig. 4 we plot ΔF_{RP} , $\Delta F_{\text{RP}}^\ddagger$, $D(z_{\text{max}})$, and $D_s(z_{\text{max}})$ as functions of θ . Fig. 4d shows clearly how sensitive $D_s(z_{\text{max}})$ is to the choice of CV. At $\theta = 90^\circ$ $D_s(z_{\text{max}})$ vanishes, since the chosen CV coincides with the ideal one. But as θ decreases, $D_s(z_{\text{max}})$ rises sharply over a narrow interval of about 10° . That is, for large θ , ∇U and $\nabla \xi$ are almost orthogonal, whereas with decreasing θ they become nearly parallel. The fall off of $D_s(z_{\text{max}})$ as θ decreases from about 45° is due to the interference of force vectors that are almost isotropically distributed, and result in essentially randomized alignment of the force and CV gradient vectors.

Since $\rho(z)$ is strongly peaked around the minima of R and P (see Fig. 3), the choices of CV in the range of 45° to 90° separate the minima well. As a consequence, ΔF_{RP} is essentially independent of the choice in this range (see Fig. 4a). In other words, over this range of choices one obtains an accurate value of the reaction free energy. Only for $\theta < 45^\circ$, where the CV begins to fail to discriminate between R and P, does the error in ΔF_{RP} set in rapidly.

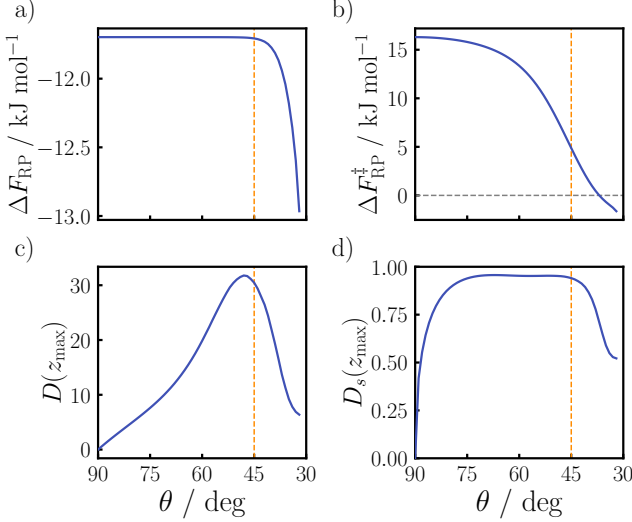


FIG. 4. Plots of a) reaction free energy ΔF_{RP} , b) activation free energy $\Delta F_{\text{RP}}^{\ddagger}$, c) orthogonality criterion $D(z_{\text{max}})$, and d) scaled criterion $D_s(z_{\text{max}})$ versus θ . Orange dashed line indicates $\theta = 45^\circ$. Gray dashed line in b) guides the eye to 0 kJ/mol.

As seen in Fig. 4b, the activation free energy is dramatically more sensitive than ΔF_{RP} to the choice of CV. It deviates from the correct value by more than “chemical accuracy” (1 kcal/mol) at $\theta \approx 60^\circ$. For $\theta < 40^\circ$, $\Delta F_{\text{RP}}^{\ddagger}$ even becomes negative. If this were correct, the rate of reaction would decrease with increasing temperature. This apparent sensitivity can be reasoned as follows. All points on the true separatrix have very low likelihood. A trial separatrix with $\theta < 90^\circ$ includes more likely configurations and therefore overestimates $\rho(z_{\text{TS}})$. Since the true $\rho(z_{\text{TS}})$ is very small, the relative error is large. For large probabilities, e.g., $\mathcal{P}(R)$, the same absolute error would incur a much smaller relative error. The relative error in the density directly translates to an absolute error in the activation free energy because of the logarithm of $\rho(z_{\text{TS}})$ (see eq. (31)).

The fact that ΔF_{RP} is largely unaffected by the choice of the CV explains why CVs based purely on chemical intuition can yield reaction free energies comparable with experiment. However, ΔF_{RP} is expected to become somewhat more sensitive to the choice of CV for more complex PES. Compared with the reaction free energy, the activation free energy is generally more sensitive. Hence, to achieve the same accuracy for $\Delta F_{\text{RP}}^{\ddagger}$ and ΔF_{RP} one must choose the CV with a great deal of care.

V. PITFALLS IN THE ESTIMATION OF THE ACTIVATION FREE ENERGY FROM THE FEP

To further illustrate the errors that one may incur by estimating $\Delta F_{\text{RP}}^{\ddagger}$ directly from the FEP alone (i.e., by invoking eq. (34)), we consider first a simple one-

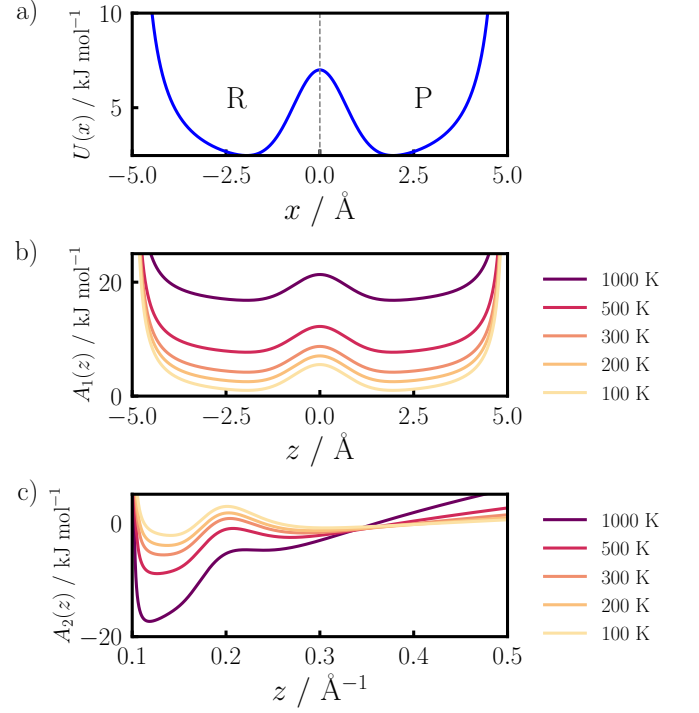


FIG. 5. a) PES $U(x)$ with $\epsilon = 5$ kJ/mol (eq. (46)); b) FEP for CV $\xi = x$ (eq. (49)); c) FEP for CV $\xi = \frac{1}{x+5}$ (eq. (50)).

dimensional model that can be treated for the most part analytically and then models of two real chemical processes.

A. One-dimensional Model

We consider a single particle of mass m moving in one dimension on the PES

$$U(x) = \epsilon \left(\frac{b}{x+5} + e^{-ax^2} - \frac{b}{x-5} \right), \quad (46)$$

where ϵ , which controls the steepness of the potential barrier, has units of kJ/mol. The parameter a , which controls the width of the barrier, is set to 1 \AA^{-2} and $b = 1 \text{ \AA}$. The PES, plotted in Fig. 5a for the case $\epsilon = 5$ kJ/mol, has two equal minima separated by a maximum at $x = 0$. Because $U(x)$ diverges as x approaches -5 or 5 , the particle is confined to the domain $-5 < x < 5$. R and P correspond, respectively, to the domains $-5 < x < 0$ and $0 < x < 5$. The symmetry of the PES dictates that $\mathcal{P}(R) = \mathcal{P}(P) = 0.5$. Therefore, from eq. (12) we get

$$k_{R \rightarrow P} = \nu / 2\mathcal{P}(R) = \nu = k_{P \rightarrow R}, \quad (47)$$

where ν is the crossing frequency. From eqs. (29) and (47), we deduce the following expression:

$$\Delta F_{\text{RP}}^{\ddagger} = -k_{\text{B}}T \ln(h\nu/k_{\text{B}}T) \quad (48)$$

TABLE I. Activation free energies (kJ mol⁻¹) for one-dimensional model PES U (eq. (46)) with $\epsilon = 5$ kJ/mol for selections of temperatures (Kelvin) and particle masses (amu). $\Delta\tilde{F}_1^\ddagger = A_1(z_{\text{TS}}) - A_1(z_{\text{R,min}})$ Letters above columns specify following differences: a) $A_2(z_{\text{TS}}) - A_2(z_{\text{R,min}})$, b) $A_2(z_{\text{max}}) - A_2(z_{\text{R,min}})$, c) $A_2(z_{\text{TS}}) - A_2(z_{\text{P,min}})$, and d) $A_2(z_{\text{max}}) - A_2(z_{\text{P,min}})$. Numbers above columns specify particle masses.

T/K	$\Delta\tilde{F}_1^\ddagger$	$\Delta\tilde{F}_2^\ddagger$				ΔF^\ddagger (eq. (30))					ΔF^\ddagger (eq. (48))*				
		a	b	c	d	1	9	25	49	100	1	9	25	49	100
100	4.53	3.77	3.78	5.09	5.10	4.50	5.41	5.84	6.12	6.42	4.49±0.10	5.48±0.13	5.90±0.29	6.12±0.27	6.22±0.26
200	4.53	3.10	3.13	5.70	5.72	5.56	7.39	8.24	8.80	9.39	5.57±0.09	7.39±0.10	8.24±0.11	8.78±0.11	9.29±0.17
300	4.53	2.50	2.55	6.35	6.40	6.98	9.72	11.00	11.84	12.73	6.97±0.08	9.67±0.06	11.02±0.12	11.83±0.06	12.79±0.16
500	4.53	1.43	1.58	7.79	7.94	10.39	14.96	17.08	18.48	19.97	10.35±0.08	14.96±0.05	17.08±0.08	18.47±0.10	19.93±0.10
1000	4.53	0.00	0.67	11.91	12.58	20.55	29.69	33.93	36.73	39.70	20.47±0.11	29.63±0.16	33.97±0.18	36.74±0.19	39.60±0.17

* ν obtained from MD by means of Heaviside function (see supplementary material)

Number after \pm -sign is standard deviation.

We compute ν by molecular dynamics (MD) simulation, as detailed in the supplementary material. MD simulations were carried out at five temperatures in the range of 100-1000 K and for five different particle masses in the range of 1-100 amu.

We consider two CVs: $\xi_1(x) = x$ and $\xi_2(x) = 1/(x+5)$. Using eq. (32), we obtain the corresponding FEPs:

$$A_1(z) = U(z) + k_B T \ln Z \quad (49)$$

$$A_2(z) = U(z^{-1} - 5) + 2k_B T \ln z + k_B T \ln Z \quad (50)$$

Setting $\epsilon = 5$ kJ/mol ensures that even the most massive particle considered crosses the dividing surface at the lowest temperature during the 10 ns time interval of the MD simulation. Figs. 5b and 5c show plots of the FEPs based on eqs. (49) and (50). We note the strong distortion of configuration space induced by $\xi_2(x)$. The domains of R and P are reversed, the minima are not equal, and the maximum of the barrier between R and P does not occur precisely at $z = 0.2$, the inverse of the position of the maximum of the barrier of the PES at $x = 0$.

Approximate activation free energies obtained according to eq. (34) are listed in Tab. I, along with “exact” values $\Delta F_{\text{RP}}^\ddagger$ obtained from eq. (30), which yields exactly the same result for both CVs, and from eq. (48) via MD. The excellent agreement between the values obtained from eqs. (30) and (48) is gratifying. According to eq. (49), $\Delta\tilde{F}_1^\ddagger$ should be independent of both temperature and particle mass. Likewise, $\Delta\tilde{F}_2^\ddagger$ should depend on temperature, but we note that by definition $\Delta\tilde{F}_2^\ddagger$ is independent of mass. Tab. I bears out these expectations.

The dominant impression of Tab. I is the severe lack of agreement between approximate and exact activation free energies. The impact of the loss of the symmetry of the PES by ξ_2 is particularly evident. Since $z_{\text{TS}} \approx z_{\text{max}}$, the results in columns a and b, which correspond to the forward reaction, agree quite well, as do those of columns c and d for the backward reaction. However, the magnitudes of the forward and backward activation free energies differ greatly. Even more noteworthy is the contrary dependence of the activation free energy on temperature. For the forward reaction it decreases with T , whereas for

TABLE II. Activation free energies (kJ mol⁻¹) for one-dimensional model PES U_1 (eq. (46)) with $\epsilon = 50$ kJ/mol for selections of temperatures (Kelvin) and particle masses (amu). $\Delta\tilde{F}_1^\ddagger = A_1(z_{\text{TS}}) - A_1(z_{\text{R,min}})$ Letters above columns specify following differences: a) $A_2(z_{\text{max}}) - A_2(z_{\text{R,min}})$ and b) $A_2(z_{\text{max}}) - A_2(z_{\text{P,min}})$. Numbers above columns specify particle masses.

T/K	$\Delta\tilde{F}_1^\ddagger$	$\Delta\tilde{F}_2^\ddagger$		ΔF^\ddagger (eq. (30))				
		a	b	1	9	25	49	100
100	45.30	44.48	45.85	44.32	45.23	45.66	45.94	46.23
200	45.30	43.68	46.40	44.50	46.33	47.18	47.74	48.33
300	45.30	42.90	46.96	45.12	47.86	49.14	49.98	50.87
500	45.30	41.38	48.09	47.12	51.69	53.81	55.21	56.70
1000	45.30	37.77	51.00	54.58	63.72	67.96	70.76	73.73

the backward reaction it increases markedly with T .

Examination of the exact data reveals the following general trends. At fixed T , $\Delta F_{\text{RP}}^\ddagger$ increases with particle mass m ; the higher T , the greater the increase. At fixed m , $\Delta F_{\text{RP}}^\ddagger$ increases with T ; the greater m , the greater the increase. Those are the same trends observed for the analytical models in Sec. III.

To see the influence of the parameter ϵ , we set $\epsilon = 50$ kJ/mol. Unbiased molecular dynamics simulations were not performed for this choice of ϵ as no barrier crossings would be observed within the previously employed simulation time. Figure S2 of the supplementary material displays plots of the PES and FEPs and Tab. II lists approximate and exact free energies of activation. In this case the immediate impression from Tab. II is the greatly improved agreement between approximate and “exact” results. Though the symmetry is still lost by ξ_2 , the distortion is relatively less severe, so that forward and backward activation energies differ less. The contrary dependence of forward and reverse activation energy on T persists, but it is relatively weaker.

The trends in $\Delta F_{\text{RP}}^\ddagger$ noted above for the case $\epsilon = 5$ kJ/mol hold for $\epsilon = 50$ kJ/mol, but the observed variations are relatively smaller. For example, whereas the change in $\Delta F_{\text{RP}}^\ddagger$ for $\epsilon = 5$ kJ/mol at $T = 300$ K is about 80% over the range of particle mass considered, it is only 13% for $\epsilon = 50$ kJ/mol. A similar observation holds for

variations of $\Delta F_{\text{RP}}^\ddagger$ with T at fixed m .

We stress that since both CVs perfectly distinguish between R and P, the computed “exact” activation free energy is identical for either, even though the CVs are very dissimilar.

B. Chemically Realistic Model - Mobility of Cu^+ in Cu-Chabazite

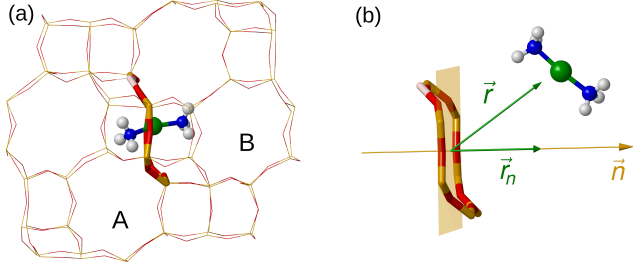


FIG. 6. (a) Migration of $\text{Cu}(\text{NH}_3)_2^+$ complex from cavity A through 8-ring window into cavity B. (b) Depiction of the CV.

We consider the realistic three-dimensional model system pictured in Fig. 6(a): a $[\text{Cu}(\text{NH}_3)_2]^+$ -complex migrating between cavities (A and B) in chabazite, a mixed crystal of the family of zeolites. This process is of importance in the deactivation of nitrogen oxides where copper-exchanged zeolites are used as catalysts.^{38–42} The migration can be regarded as a “chemical reaction”, in which the Cu-complex in cavity A or B is the “reactant” or “product”, respectively. The reaction consists of the complex diffusing out of cavity A through the 8-ring (8 silicon sites) window and into cavity B. Millan *et al.*⁴³ have simulated this system by means of *ab initio* MD combined with umbrella sampling (for details see Ref. 43). The CV they employ, which is depicted in Fig. 6(b), is defined with respect to the 8-ring window that separates the cavities. It is the projection of the vector position of the Cu atom onto the normal to the “average” plane of the central 4 Si and 2 O atoms of the ring that remain nearly in the same plane.

Our primary purpose is to analyze the data of Millan *et al.*⁴³ in order to determine the exact values of the reaction free energy and activation free energy for the migration reaction described above. We are especially interested in the effect of mass on the activation free energy. The authors of Ref. 43 supplied the coordinates of the trajectories and the bias used for the umbrella sampling for every frame. We implemented the CV in pyTorch⁴⁴ to gain easy access to $\nabla\xi$, and consequently m_ξ^{-1} (see eq. (27)), through the automatic differentiation in Torch. We computed the weights of every frame with an in-house implementation of MBAR.⁴⁵ The weights were used to re-compute the FEP and compare it with the result of Millan *et al.*⁴³, as well as to compute the conditional ensemble average of m_ξ^{-1} needed for the

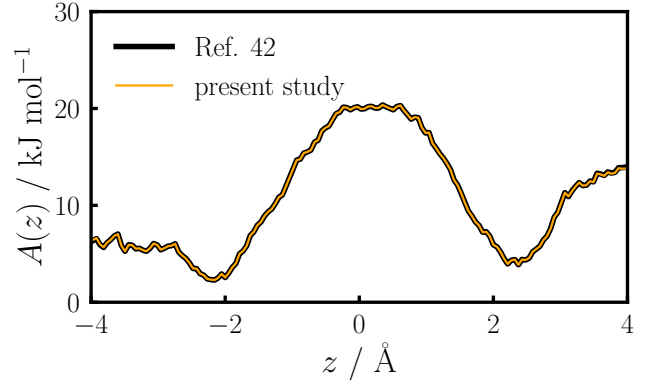


FIG. 7. Comparison of FEP obtained in present study with that reported in Ref. 43.

TABLE III. Comparison of approximate and exact free energies (in kJ mol^{-1}).

	$z_{\text{TS}}/\text{\AA}$	ΔF_{AB}	$\Delta \tilde{F}_{\text{AB}}$	$\Delta F_{\text{AB}}^\ddagger$	$\Delta \tilde{F}_{\text{AB}}^\ddagger$
Ref. 43	0.35	—	1.5	—	17
present study	0.35	2.8	1.6	26.2	18.1
present study	0.00	2.8	1.6	25.8	17.6

calculation of $\langle \lambda_\xi \rangle_{z_{\text{TS}}}$ (see eq. (30)).

The FEPs are plotted in Fig. 7, which shows that the agreement of our FEP with that of Millan *et al.*⁴³ is excellent. The probability densities are normalized according to $\int_{-4}^4 dz e^{-\beta A(z)} = 1$. Millan *et al.*⁴³ take the maximum of $A(z)$, located at $z = 0.35 \text{ \AA}$, to be the position of the TS. According to the definition of the CV, the TS should be at $z = 0.0 \text{ \AA}$. We computed exact and approximate reaction and activation free energies for both choices of the TS. Tab. III shows very clearly the large influence of mass on the activation free energy. Further, the approximate free energies ($\Delta \tilde{F}_{\text{AB}}$ and $\Delta \tilde{F}_{\text{AB}}^\ddagger$) obtained by us agree well with those of Millan *et al.*⁴³. The precise choice of z_{TS} has little effect on the activation free energies, because the FEP is quite flat around $z = 0$.

Since Millan *et al.*⁴³ used the same CV for all of the systems they simulated, the correction of the activation free energy should be about the same for all. Therefore the correction should not affect the ordering of the barriers ($\Delta \tilde{F}_{\text{AB}}^\ddagger$) they determined approximately. However, we would expect any comparison with experimental activation barriers to depend strongly on the difference between the approximate and exact treatments.

C. Chemically Realistic Model - Radical Cyclization

As a second chemical example, we consider the intramolecular cyclization of the 5-hexenyl radical (see Fig. 8), a radical clock reaction.⁴⁶ The forward reaction involves the formation of a new single bond and the conversion of a C-C double bond to a single bond.

Carbon single bonds are usually stiff and have high activation barriers, as reflected in the experimental activation free energy for the cyclization, $\Delta F_{\text{exp}}^\ddagger(300 \text{ K}) = 42 \pm 4 \text{ kJ/mol}$.⁴⁷ Hence, we expect the approximate relation in eq. (34) to hold. As CV we choose the distance between the two carbon atoms (C1 and C5) that form a new bond, $\xi = d(\text{C1} - \text{C5})$. The associated mass m_ξ is constant and equal to the reduced mass of the two carbon atoms (i.e., 6 amu).

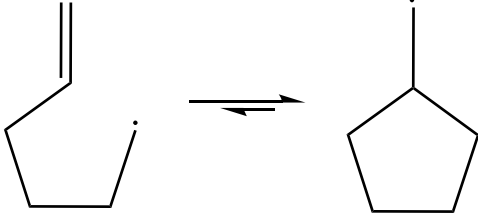


FIG. 8. Scheme of the intramolecular cyclization of the reactant 5-hexenyl radical to the product methylcyclopentane radical.

The system was simulated at 300 K by means of *ab initio* MD at the $\omega\text{B97M-V/def2-TZVP}$ ^{48,49} level of theory and solvated in benzene with the COSMO continuum solvation model.⁵⁰ We employed WTM-eABF^{51–53} as enhanced sampling algorithm. The unbiased weights were recovered with the recently developed combination of eABF and MBAR.⁵⁴ Details of the simulation are given in the supplementary material.

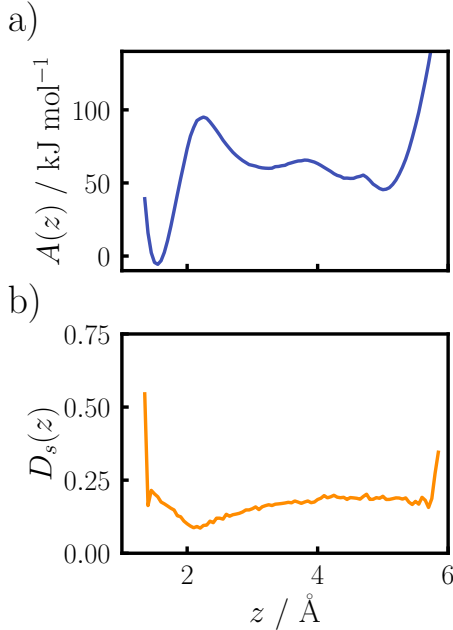


FIG. 9. a) Free energy profile for the reaction shown in Fig. 8. b) Orthogonality measure $D_s(z)$.

The FEP (Fig. 9a) shows one deep minimum for P (methylcyclopentane radical) and three shallow minima

for R (5-hexenyl radical). We take all configurations with $z > 2.2 \text{ Å}$ to belong to R. The scaled orthogonality measure D_s (eq. (45), Fig. 9b) is lower than 0.25 for almost the entire range of z values, rising sharply only at the ends of the simulated range. The plot of D_s shows a clear local minimum near the local maximum of the FEP, indicating that it is a good CV.

In Tab. IV we can see that the exact reaction and activation free energies obtained from eqs. (42) and (30), respectively, agree well with the approximate ones. Hence, this example confirms that eq. (34) does hold in cases of high barriers, low temperatures, light CVs, and narrow wells about the minima of R and P on the PES.

TABLE IV. Comparison of approximate and exact free energies (in kJ mol^{-1}) for the reaction shown in Fig. 8

ΔF_{RP}	$\Delta \tilde{F}_{\text{RP}}$	$\Delta F_{\text{RP}}^\ddagger$	$\Delta \tilde{F}_{\text{RP}}^\ddagger$	$\Delta F_{\text{PR}}^\ddagger$	$\Delta \tilde{F}_{\text{PR}}^\ddagger$
-49.1	-51.1	48.2	49.7	97.3	100.7

VI. DISCUSSION AND CONNECTION TO PRIOR WORK

This study is not the first work to present expressions for the rate constant and activation free energy based on transition state theory.^{29–34,55} However, previous work often lacks a stepwise derivation of their expression for the rate constant. Further, Refs. 55 and 34, which also present equations for the activation free energy, still include local differences of the FEP in their final expressions, which can thus be interpreted as corrections to the approximate treatment. Because of complex notation it is difficult to verify whether their expressions are equivalent to our eq. (30). It is perhaps due to the complexity of the equations and lack of physical interpretability that their expressions have not been widely adopted. Therefore, we are motivated to present a meticulous and straightforward derivation of the exact formula (eq. (30)) for the activation free energy $\Delta F_{\text{RP}}^\ddagger$ for the two-state process from a reactant R to a product P in a novel form. The formula involves three key quantities having clear physical interpretations. Two of these, $\rho(z_{\text{TS}})$ and $\mathcal{P}(\text{R}) = \int_{\Omega_{\text{R}}} dz \rho(z)$, depend only on $\rho(z)$, the marginal probability density that the CV $\xi(\mathbf{x})$ takes the value z . The third, $\langle \lambda_\xi \rangle_{z_{\text{TS}}}$, can be rewritten as $\sqrt{h^2/2\pi k_{\text{B}}T} \left\langle \sqrt{m_\xi^{-1}} \right\rangle_{z_{\text{TS}}}$ to indicate explicitly the dependence on the effective mass of the pseudo-particle associated with the CV. The three clearly defined terms also facilitate implementation.

The presence of the factor $\left\langle \sqrt{m_\xi^{-1}} \right\rangle_{z_{\text{TS}}}$ in the exact formula for $k_{\text{R} \rightarrow \text{P}}$ (eq. (28)) shows that knowledge of $\rho(z)$ (or alternatively $A(z)$) alone is insufficient to determine the rate constant $k_{\text{R} \rightarrow \text{P}}$. We note that in the “conventional” transition state theory³⁶ the rate constant is expressed in terms of canonical partition functions for reac-

tant and activated complex (minus that associated with the CV (reaction coordinate)) and the discrete masses of the atoms enter into them. In the present treatment the effective mass m_ξ depends not only on the discrete masses of atoms but also on the gradient of the CV (see eq. (27)). If the CV is linear in the Cartesian coordinates, then $\left\langle \sqrt{m_\xi^{-1}} \right\rangle_{z_{\text{TS}}}$ is readily expressible explicitly in terms of the discrete masses.⁵⁶ In general, however, the CV-conditioned ensemble average must be computed.

The “gauge-independent geometric” free-energy profile, given by

$$\begin{aligned} A^G(z) &= -k_B T \ln [\rho(z) \langle |\nabla_{\mathbf{x}} \xi| \rangle_z] \\ &= -k_B T \ln \left[\rho(z) \left\langle \sqrt{m_\xi^{-1}} \right\rangle_z \right]. \end{aligned} \quad (51)$$

has been proposed^{24,25} as an alternative to the “standard” FEP (eq. (32)). Since the geometric FEP at the transition point is related to $\Delta F_{\text{RP}}^\ddagger$ according to

$$\begin{aligned} A^G(z_{\text{TS}}) - k_B T \ln \sqrt{\frac{h^2}{2\pi k_B T}} &= -k_B T \ln [\rho(z_{\text{TS}}) \langle \lambda_\xi \rangle_{\text{TS}}] \\ &= \Delta F_{\text{RP}}^\ddagger - k_B T \ln \mathcal{P}(\text{R}), \end{aligned} \quad (52)$$

it is also referred to as the “kinetic” free-energy profile.⁵⁷ On one hand, like $A(z)$, $A^G(z)$ cannot alone provide $\Delta F_{\text{RP}}^\ddagger$. On the other, unlike $A(z)$, $A^G(z)$ cannot alone furnish ΔF_{RP} . The essential reason is that $e^{-\beta A^G(z)}$ is generally not a probability density, whereas $e^{-\beta A(z)}$ always is.

We remark on an apparent inconsistency in the dimensions of terms in eq. (31), as noted in Ref. 57. We observe that the dimensions of $\rho(z)$ are those of ξ^{-1} and the dimensions of $\langle \lambda_\xi \rangle$ are those of ξ . The argument of the logarithm is therefore dimensionless, as it should be. Thus, there is no inconsistency. It appears only because of the tendency to overlook that the definition of the FEP includes an implicit scaling factor, which is unfortunately rarely, if ever, pointed out. The same remarks apply as well to the geometric FEP.

VII. CONCLUSION

Our applications of the exact formula for the activation free energy demonstrate how significant errors can arise when $\Delta F_{\text{RP}}^\ddagger$ is approximated simply by the difference between the values of the FEP at the transition state and reactant.

The often employed procedure to obtain $\Delta F_{\text{RP}}^\ddagger$ solely from the FEP (by taking the difference between the values at the transition state and reactant (eq. (34))) is an approximation. If $\rho(z)$ is strongly peaked in the vicinity of the minimum of R (i.e., at low temperature and small effective mass m_ξ), then eq. (34) may be satisfactory (see

Section V C). However, it is especially questionable when the temperature is high, m_ξ is large, and the barrier of the PES between R and P is low (see Section V B).

The exact formula for $\Delta F_{\text{RP}}^\ddagger$ (eq. (30)) assumes implicitly that the CV is good (i.e., it is orthogonal to the separatrix). According to our study of the two-dimensional model PES with a systematically variable CV, as the CV becomes less good the reliability of $\Delta F_{\text{RP}}^\ddagger$ decreases markedly, while that of the reaction free energy ΔF_{RP} is only slightly affected. We conclude that one must choose the CV with considerable caution in order to achieve the same accuracy for both kinetic and thermodynamic properties.

The exact formulas for $\Delta F_{\text{RP}}^\ddagger$ (eq. (30)) and ΔF_{RP} (eq. (42)) depend only on CV-conditioned ensemble averages, which are readily available from enhanced-sampling simulations via reweighting techniques.^{45,54,58–63} Therefore, it should be more convenient to use these formulas than to resort to alternative special sampling strategies such as infrequent metadynamics.^{64,65}

In light of the results of the present study and those of our prior work²³, we recommend less reliance on the FEP alone and more on the exact formulas, which can be easily evaluated from data provided by commonly employed advanced-sampling algorithms. The exact formulas are more reliable and can be clearly related to experimental data. In this regard we agree with Ref. 34 that use of the FEP alone should be discouraged, except we think that $\Delta F_{\text{RP}}^\ddagger$ is a better touchstone for comparison between theory and experiment than the rate constant itself.

SUPPLEMENTARY MATERIAL

The supplementary material contains the following: (1) proof that eq. (14) yields the frequency of crossing the dividing surface; (2) proof of the equivalency of eqs. (12) and (13); (3) analytical one-dimensional models of Section III; (4) computational details of Section IV; (5) computation of the frequency of crossing the dividing surface; (6) plots of the FEPs for models of Section V A with large ϵ ; (7) computational details of Section V C.

ACKNOWLEDGMENTS

The authors thank Dr. Reisel Millan, who provided full access to their simulations of chabazite and furnished Fig. 6. J.C.B.D. is thankful for the support of the Leopoldina Fellowship Program, German National Academy of Sciences Leopoldina, grant number LPDS 2021-08. C.O. acknowledges financial support by the “Deutsche Forschungsgemeinschaft” (DFG, German Research Foundation) within cluster of excellence “e-conversion” (EXC 2089/1-390776260) and SFB 1309-325871075 “Chemical Biology of Epigenetic Modifications” and further support as Max-Planck-Fellow at

the MPI-FKF Stuttgart. R.G.-B. acknowledges support from the Jeffrey Cheah Career Development Chair.

AUTHOR DECLARATIONS

Conflict of Interest

The authors have no conflicts of interest to disclose.

DATA AVAILABILITY STATEMENT

The data that support the findings of this study are available from the corresponding author upon reasonable request.

REFERENCES

- ¹P. Kollman, *Chem. Rev.* **93**, 2395 (1993).
- ²C. Chipot and A. Pohorille, eds., *Free Energy Calculations* (Springer-Verlag, Berlin Heidelberg, 2007).
- ³C. D. Christ, A. E. Mark, and W. F. Van Gunsteren, *J. Comput. Chem.* **31**, 1569 (2009).
- ⁴C. Chipot, *WIREs Comput. Mol. Sci.* **4**, 71 (2014).
- ⁵N. Hansen and W. F. Van Gunsteren, *J. Chem. Theory Comput.* **10**, 2632 (2014).
- ⁶R. E. Skyner, J. L. McDonagh, C. R. Groom, T. van Mourik, and J. B. O. Mitchell, *Phys. Chem. Chem. Phys.* **17**, 6174 (2015).
- ⁷D. L. Mobley and M. K. Gilson, *Annu. Rev. of Biophys.* **46**, 531 (2017).
- ⁸P. G. Bolhuis, C. Dellago, and D. Chandler, *Proc. Nat. Acad. Sci. USA* **97**, 5877 (2000).
- ⁹D. Mendels, G. Piccini, and M. Parrinello, *J. Phys. Chem. Lett.* **9**, 2776 (2018).
- ¹⁰Y. Wang, J. M. L. Ribeiro, and P. Tiwary, *Nat. Commun.* **10** (2019).
- ¹¹L. Sun, J. Vandermause, S. Batzner, Y. Xie, D. Clark, W. Chen, and B. Kozinsky, *J. Chem. Theory Comput.* **18**, 1549 (2022).
- ¹²L. Bonati, V. Rizzi, and M. Parrinello, *J. Phys. Chem. Lett.* **11**, 2998 (2020).
- ¹³D. Wang and P. Tiwary, *J. Chem. Phys.* **154** (2021).
- ¹⁴W. L. Jorgensen, *J. Amer. Chem. Soc.* **111**, 3770 (1989).
- ¹⁵J. P. Valleau and T. J.M., *J. Comput. Phys.* **23**, 187 (1977).
- ¹⁶E. Darve and A. Pohorille, *J. Chem. Phys.* **115**, 9169 (2001).
- ¹⁷A. Laio and M. Parrinello, *Proc. Natl. Acad. Sci. USA* **99**, 12562 (2002).
- ¹⁸C. Abrams and G. Bussi, *Entropy* **16**, 163 (2014).
- ¹⁹V. Spiwok, Z. Sucer, and P. Hosek, *Biotechnol. Adv.* **33**, 1130 (2015).
- ²⁰O. Valsson, P. Tiwary, and M. Parrinello, *Annu. Rev. Phys. Chem.* **67**, 159 (2016).
- ²¹P. G. Bolhuis, D. Chandler, C. Dellago, and P. L. Geissler, *Annu. Rev. Phys. Chem.* **53**, 291 (2002).
- ²²N. V. Plotnikov, S. C. Kamerlin, and A. Warshel, *Journal of Physical Chemistry B* **115**, 7950 (2011).
- ²³J. C. B. Dietschreit, D. J. Diestler, and C. Ochsenfeld, *J. Chem. Phys.* **156**, 114105 (2022).
- ²⁴C. Hartmann and C. Schütte, *Physica D* **228**, 59 (2007).
- ²⁵C. Hartmann, J. C. Latorre, and G. Ciccotti, *EPJ Special Topics* **200**, 73 (2011).
- ²⁶M. Fixman, *Proc. Natl. Acad. Sci. USA* **71**, 3050 (1974).
- ²⁷K. den Otter, *J. Chem. Phys.* **112**, 7283 (2000).
- ²⁸W. K. den Otter, *J. Chem. Theory Comput.* **9**, 3861 (2013).
- ²⁹B. J. Berne, M. Borkovec, and J. E. Straub, *J. Phys. Chem.* **92**, 3711 (1988).
- ³⁰E. A. Carter, G. Ciccotti, J. T. Hynes, and R. Kapral, *Chem. Phys. Lett.* **156**, 472 (1989).
- ³¹P. Hänggi, P. Talkner, and M. Borkovec, *Rev. Mod. Phys.* **62**, 251 (1990).
- ³²K. Hinsen and B. Roux, *J. Chem. Phys.* **106**, 3567 (1997).
- ³³T. Bučko, S. Chibani, J. F. Paul, L. Cantrel, and M. Badawi, *Phys. Chem. Chem. Phys.* **19**, 27530 (2017).
- ³⁴S. Bailleul, K. Dedeker, P. Cnudde, L. Vanduyfhuys, M. Waroquier, and V. Van Speybroeck, *J. Catal.* **388**, 38 (2020).
- ³⁵E. Vanden-Eijnden and F. A. Tal, *J. Chem. Phys.* **123**, 184103 (2005).
- ³⁶K. J. Laidler, "Chemical kinetics," (Harper and Row, 1987) Chap. 4.
- ³⁷M. A. Murcko, H. Castejon, and K. B. Wiber, *J. Phys. Chem.* **100**, 16162 (1996).
- ³⁸J. H. Kwak, R. G. Tonkyn, D. H. Kim, J. Szanyi, and C. H. Peden, *J. Catal.* **275**, 187 (2010).
- ³⁹F. Gao, J. H. Kwak, J. Szanyi, and C. H. F. Peden, *Topics in Catalysis* **56**, 1441 (2013).
- ⁴⁰N. Martín, C. R. Boruntea, M. Moliner, and A. Corma, *Chem. Commun.* **51**, 11030 (2015).
- ⁴¹E. Borfecchia, P. Beato, S. Svelle, U. Olsbye, C. Lamberti, and S. Bordiga, *Chem. Soc. Rev.* **47**, 8097 (2018).
- ⁴²C. H. Peden, *J. Catal.* **373**, 384 (2019).
- ⁴³R. Millan, P. Cnudde, V. van Speybroeck, and M. Boronat, *JACS Au* **1**, 1778 (2021).
- ⁴⁴A. Paszke, S. Gross, F. Massa, A. Lerer, J. Bradbury, G. Chanan, T. Killeen, Z. Lin, N. Gimeshain, L. Antiga, A. Desmaison, A. Kopf, E. Yang, Z. DeVito, M. Raison, A. Tejani, S. Chilamkurthy, B. Steiner, L. Fang, J. Bai, and S. Chintala, in *Advances in Neural Information Processing Systems 32* (Curran Associates, Inc., 2019) pp. 8024–8035.
- ⁴⁵M. R. Shirts and J. D. Chodera, *J. Chem. Phys.* **129**, 1 (2008).
- ⁴⁶D. Griller and K. U. Ingold, *Acc. Chem. Res.* **13**, 317 (1980).
- ⁴⁷C. Chatgililoglu, J. Dickhaut, and B. Giese, *J. Org. Chem.* **56**, 6399 (1991).
- ⁴⁸N. Mardirossian and M. Head-Gordon, *J. Chem. Phys.* **142**, 074111 (2015).
- ⁴⁹A. Schäfer, H. Horn, and R. Ahlrichs, *J. Chem. Phys.* **97**, 2571 (1992).
- ⁵⁰A. Klamt and G. J. G. J. Schuurmann, *J. Chem. Soc., Perkin Trans. 2*, 799 (1993).
- ⁵¹A. Lesage, T. Lelievre, G. Stoltz, and J. Henin, *J. Phys. Chem. B* **121**, 3676 (2017).
- ⁵²H. Fu, H. Zhang, H. Chen, X. Shao, C. Chipot, and W. Cai, *J. Phys. Chem. Lett.* **9**, 4738 (2018).
- ⁵³H. Fu, X. Shao, W. Cai, and C. Chipot, *Acc. Chem. Res.* **52**, 3254 (2019).
- ⁵⁴A. Hulm, J. C. B. Dietschreit, and C. Ochsenfeld, *J. Chem. Phys.* **157**, 024110 (2022).
- ⁵⁵G. K. Schenter, B. C. Garrett, and D. G. Truhlar, *J. Chem. Phys.* **119** (2003).
- ⁵⁶E. Neria, S. Fischer, and M. Karplus, *J. Chem. Phys.* **105**, 1902 (1996).
- ⁵⁷K. M. Bal, S. Fukuhara, Y. Shibuta, and E. C. Neyts, *J. Chem. Phys.* **153** (2020).
- ⁵⁸S. Kumar, J. M. Rosenberg, D. Bouzida, R. H. Swendsen, and P. A. Kollman, *J. Comput. Chem.* **13**, 1011 (1992).
- ⁵⁹G. Tian, *Eur. Phys. J. B* **63**, 235 (2008).
- ⁶⁰M. Bonomi, A. Barducci, and M. Parrinello, *J. Comput. Chem.* **30**, 1615 (2009).
- ⁶¹P. Tiwary and M. Parrinello, *J. Phys. Chem. B* **119**, 736 (2015).
- ⁶²T. M. Schäfer and G. Settanni, *J. Chem. Theory Comput.* **16**, 2042 (2020).
- ⁶³M. R. Shirts and A. L. Ferguson, *J. Chem. Theory Comput.* **16**, 4107 (2020).
- ⁶⁴A. Dickson, P. Tiwary, and H. Vashisth, *Curr. Topics Med. Chem.* **17**, 2626 (2017).

- ⁶⁵P. Cossio, *Biophysical Journal* **121**, 5a (2022).
- ⁶⁶C. Cohen-Tannoudji, B. Diu, and F. Lal  , *Quantum Mechanics* (John Wiley and Sons, New York, 1977).
- ⁶⁷C. R. Harris, K. J. Millman, S. J. van der Walt, R. Gommers, P. Virtanen, D. Cournapeau, E. Wieser, J. Taylor, S. Berg, N. J. Smith, R. Kern, M. Picus, S. Hoyer, M. H. van Kerkwijk, M. Brett, A. Haldane, J. F. del R  o, M. Wiebe, P. Peterson, P. G  rard-Marchant, K. Sheppard, T. Reddy, W. Weckesser, H. Abbasi, C. Gohlke, and T. E. Oliphant, *Nature* **585**, 357 (2020).
- ⁶⁸J. D. Hunter, *Computing in Science & Engineering* **9**, 90 (2007).
- ⁶⁹J. Kussmann and C. Ochsenfeld, *J. Chem. Phys.* **138**, 134114 (2013).
- ⁷⁰J. Kussmann and C. Ochsenfeld, *J. Chem. Theory Comput.* **11**, 918 (2015).
- ⁷¹H. Laqua, T. H. Thompson, J. Kussmann, and C. Ochsenfeld, *J. Chem. Theory Comput.* **16**, 1456 (2020).
- ⁷²H. Laqua, J. Kussmann, and C. Ochsenfeld, *J. Chem. Phys.* **154**, 214116 (2021).
- ⁷³N. Mardirossian and M. Head-Gordon, *J. Chem. Phys.* **144**, 214110 (2016).

Supporting Material for: From Free-Energy Profiles to Activation Free Energies

Appendix A: Proof that Eq. (14) Yields the Frequency of Crossing the Dividing Surface

Starting with eq. (14) of the article,

$$\nu = \lim_{\tau \rightarrow \infty} \frac{1}{\tau} \int_0^\tau dt \left| \frac{d}{dt} \Theta[\xi(\mathbf{x}(t)) - z_{\text{TS}}] \right|, \quad (\text{A1})$$

we apply the chain rule of differentiation to obtain

$$\begin{aligned} \nu &= \lim_{\tau \rightarrow \infty} \frac{1}{\tau} \int_0^\tau dt \left| \frac{d\Theta}{d\xi} \dot{\xi}(t) \right| \\ &= \lim_{\tau \rightarrow \infty} \frac{1}{\tau} \int_0^\tau dt \left| \frac{d\Theta}{d\xi} \right| |\dot{\xi}(t)| \\ &= \lim_{\tau \rightarrow \infty} \frac{1}{\tau} \int_0^\tau dt |\delta[\xi(t) - z_{\text{TS}}]| |\dot{\xi}(t)| \end{aligned} \quad (\text{A2})$$

We now utilize the property of the Dirac distribution⁶⁶

$$\delta[f(t)] = \sum_i \frac{\delta(t - t_i)}{|(df/dt)_{t=t_i}|}, \quad (\text{A3})$$

where $f(t_i) = 0$ and $(df/dt)_{t=t_i} \neq 0$, to recast eq. (A2) as

$$\begin{aligned} \nu &\lim_{\tau \rightarrow \infty} \frac{1}{\tau} \int_0^\tau dt \left(\sum_i \frac{\delta(t - t_i)}{|\dot{\xi}(t_i)|} |\dot{\xi}(t)| \right) \\ &= \lim_{\tau \rightarrow \infty} \frac{1}{\tau} \sum_i \frac{1}{|\dot{\xi}(t_i)|} \int_0^\tau dt \delta(t - t_i) |\dot{\xi}(t)| \\ &= \lim_{\tau \rightarrow \infty} \frac{1}{\tau} \sum_{j=1}^{N_\tau} 1 \\ &= \lim_{\tau \rightarrow \infty} \frac{N_\tau}{\tau} \end{aligned} \quad (\text{A4})$$

where N_τ is the number of zeroes of $\xi(t) - z_{\text{TS}}$ on the interval $[0, \tau]$, which is equal to the number of times $\xi(t) - z_{\text{TS}}$ changes sign during the interval. Hence, N_τ/τ is just the frequency of crossing the dividing surface.

Appendix B: Proof of the Equivalency of Eqs. (12) and (13)

We assume that in general the CV is “good” in that it distinguishes properly between R and P (i.e., no configuration of R has the same value of the CV as a configuration of P). Moreover, implicit in eq. (13) is the assumption that the value of $z_{\text{TS}} - \xi(\mathbf{x})$ is positive for

configurations of R and negative for those of P. It follows that

$$\langle \Theta[z_{\text{TS}} - \xi(\tilde{\mathbf{x}})] \rangle_{p,q} = \mathcal{P}(\text{R}), \quad (\text{B1})$$

where the Heaviside function is 1 in the domain of R, where its argument is positive.

Assuming the system to be ergodic, we can replace the time average in eq. (S2) with the ensemble average

$$\nu = \left\langle \delta[\xi(\tilde{\mathbf{x}}) - z_{\text{TS}}] \left| \dot{\xi}(\tilde{\mathbf{x}}) \right| \right\rangle_{p,q}. \quad (\text{B2})$$

We note that since ν is the frequency of crossings due to both forward and reverse reactions, the absolute value of the rate of change of the CV is necessary to prevent cancellations of forward and reverse contributions. Further, because the system is taken to be in thermodynamic equilibrium, the forward and reverse reactions occur with the same frequency. Hence, we can simply count reactions in one direction, say forward from R to P, where $\dot{\xi} > 0$. Then the absolute value of $\dot{\xi}$ becomes unnecessary. The sign of the velocity is enforced by introducing a Heaviside function. Thus, we have

$$\nu/2 = \left\langle \delta[\xi(\tilde{\mathbf{x}}) - z_{\text{TS}}] \dot{\xi}(\tilde{\mathbf{x}}) \Theta(\dot{\xi}) \right\rangle_{p,q} \quad (\text{B3})$$

This is precisely the numerator of the expression in eq. (13) in the article. Dividing eq. (S7) by (S5) finally gives

$$\frac{\nu}{2\mathcal{P}(\text{R})} = \frac{\left\langle \delta[\xi(\tilde{\mathbf{x}}) - z_{\text{TS}}] \dot{\xi}(\tilde{\mathbf{x}}) \Theta(\dot{\xi}) \right\rangle_{p,q}}{\langle \Theta[z_{\text{TS}} - \xi(\tilde{\mathbf{x}})] \rangle_{p,q}} \quad (\text{B4})$$

Appendix C: Analytical One-Dimensional Models of Section III

Here we treat a one-dimensional system consisting of a single particle of mass m moving on a PES with two minima separated by a maximum. We consider two model PESs, comparing the approximate and “exact” free energies of activation.

We take the PES of the first to be a square well specified piecewise by

$$U_{\text{SW}}(x) = \begin{cases} \infty, & x < 0 \\ \epsilon_{\text{R}}, & 0 < x < L_{\text{R}} - \delta \\ \epsilon_{\text{B}}, & L_{\text{R}} - \delta < x < L_{\text{R}} + \delta \\ \epsilon_{\text{P}}, & L_{\text{R}} + \delta < 0 < L \\ \infty, & L < x \end{cases} \quad (\text{C1})$$

Assuming that $\delta \ll L$, $\epsilon_{\text{B}} > \epsilon_{\text{R}}$, and $\epsilon_{\text{B}} > \epsilon_{\text{P}}$, and taking the CV to be $\xi(x) = x$, we derive the probability density

$$\rho_{\text{SW}}(z) = Z^{-1} e^{-\beta U_{\text{SW}}(z)}. \quad (\text{C2})$$

Hence the probability of observing R is

$$\mathcal{P}_{\text{SW}}(\text{R}) = \int_{0_{\text{R}}} dz \rho_{\text{SW}}(z) = Z^{-1} L_{\text{R}} e^{-\beta \epsilon_{\text{R}}} \quad (\text{C3})$$

According to eq. (30), we have for the “exact” free energy of activation

$$\begin{aligned}\Delta F_{\text{SW}}^\ddagger &= -k_B T \ln \left[\frac{\rho_{\text{SW}}(z_{\text{TS}}) \langle \lambda_\xi \rangle_{z_{\text{TS}}}}{\mathcal{P}_{\text{SW}}(\mathbf{R})} \right] \\ &= -k_B T \ln \left[\frac{e^{-\beta \epsilon_B}}{Z} \frac{Z}{L_R e^{-\beta \epsilon_R}} \langle \lambda_\xi \rangle_{z_{\text{TS}}} \right] \\ &= \epsilon_B - \epsilon_R - k_B T \ln \left[\sqrt{h^2/2\pi m k_B T L_R^2} \right], \quad (\text{C4})\end{aligned}$$

where we use the relation $\langle \lambda_\xi \rangle_{z_{\text{TS}}} = \sqrt{h^2/2\pi m k_B T}$.

For the second model we consider a double-well PES having minima of ϵ_R at $x_{R,\min}$ and ϵ_P at $x_{P,\min}$, separated by a maximum of ϵ_B at the transition state. We approximate this PES about the minima by the harmonic-oscillator (HO) approximation (e.g., $U(x) \approx U_{\text{HO}}(x) = \epsilon_R + k/2(x - x_{R,\min})^2$, where the force constant is $k = \left. \frac{d^2 U}{dx^2} \right|_{x=x_{R,\min}}$). We again take the CV to be $\xi(x) = x$. Thus, the probability of observing \mathbf{R} is

$$\begin{aligned}\mathcal{P}(\mathbf{R}) &= \int_{\Omega_R} dz e^{-\beta U(z)} Z^{-1} \\ &\approx Z^{-1} \int_{-\infty}^{\infty} dx e^{-\beta(\epsilon_R + \frac{k}{2}(x - x_{R,\min})^2)} \\ &= \frac{e^{-\beta \epsilon_R}}{Z} \sqrt{\frac{2\pi}{k\beta}}, \quad (\text{C5})\end{aligned}$$

where we approximate the probability density in the domain of \mathbf{R} by $\rho_{\text{HO}}(\xi) = Z^{-1} e^{-\beta U_{\text{HO}}(x)}$. Using eq. (30), we obtain the “exact” activation free energy

$$\begin{aligned}\Delta F_{\text{HO}}^\ddagger &= -k_B T \ln \left[\frac{\rho_{\text{HO}}(z_{\text{TS}}) \langle \lambda_\xi \rangle_{z_{\text{TS}}}}{\mathcal{P}_{\text{HO}}(\mathbf{R})} \right] \\ &= -k_B T \ln \left[\frac{e^{-\beta \epsilon_B}}{Z} \frac{Z}{e^{-\beta \epsilon_R}} \sqrt{\frac{k}{2\pi k_B T}} \sqrt{h^2/2\pi m k_B T} \right] \\ &= \epsilon_B - \epsilon_R - k_B T \ln \sqrt{h^2 k / [(2\pi k_B)^2 m T^2]} \quad (\text{C6})\end{aligned}$$

where we again invoke the relation $\langle \lambda_\xi \rangle_{z_{\text{TS}}} = \sqrt{h^2/2\pi m k_B T}$.

According to eq. (34), the approximate activation free energy for both models is given by:

$$\begin{aligned}\Delta \tilde{F}^\ddagger &= A(z_{\text{TS}}) - A(z_{R,\min}) = k_B T \ln \frac{\rho(z_{\text{TS}})}{\rho(z_{R,\min})} \\ &= U(z_{\text{TS}}) - U(z_{R,\min}) = \epsilon_B - \epsilon_R \quad (\text{C7})\end{aligned}$$

for both models. Comparing eq. (C7) with eq. (C4) and with eq. (C6), we see that the difference between “exact” and approximate activation free energies is, respectively

$$\text{corr}_{\text{SW}} = \Delta F_{\text{SW}}^\ddagger - \Delta \tilde{F}^\ddagger = k_B T \ln \left[\sqrt{2\pi k_B T m L_R^2 / h^2} \right] \quad (\text{C8})$$

$$\text{corr}_{\text{HO}} = \Delta F_{\text{HO}}^\ddagger - \Delta \tilde{F}^\ddagger = k_B T \ln \left[\sqrt{(2\pi)^2 k_B^2 T^2 m / h^2 k} \right]. \quad (\text{C9})$$

Appendix D: Computational Details of Section IV

Required numerical computations are handled by NumPy⁶⁷. Plots are generated with Matplotlib⁶⁸.

1. Determination of the Parameter a

The CV in Section IV of the article is given by eq. (40)

$$\xi(x, y) = ax + (1 - a)y, \quad (\text{D1})$$

where a is restricted to the interval $[0, 1]$. It is determined by specifying the angle θ between $\nabla \xi$ and \mathbf{e}_S , the unit vector parallel with the true separatrix \mathcal{S} (i.e., \mathbf{e}_y). The angle is related to the two vectors by

$$\cos \theta = \frac{\nabla \xi}{|\nabla \xi|} \cdot \mathbf{e}_S, \quad (\text{D2})$$

where θ is restricted to the interval $[0, \pi/2]$. From eq. (D1) we obtain

$$\nabla \xi = a\mathbf{e}_x + (1 - a)\mathbf{e}_y. \quad (\text{D3})$$

Substitution of eq. (D3) into eq. (D2) yields

$$\cos \theta = \frac{a\mathbf{e}_x + (1 - a)\mathbf{e}_y}{\sqrt{a^2 + (1 - a)^2}} \cdot \mathbf{e}_y = \frac{(1 - a)}{\sqrt{a^2 + (1 - a)^2}}. \quad (\text{D4})$$

Solving this equation for a , we get

$$a_{\pm} = \frac{\sin^2 \theta}{\sin^2 \theta - \cos^2 \theta} \pm \sqrt{\frac{\sin^4 \theta}{(\sin^2 \theta - \cos^2 \theta)^2} - \frac{\sin^2 \theta}{\sin^2 \theta - \cos^2 \theta}} \quad (\text{D5})$$

We observe that this formula breaks down if $\sin \theta = \cos \theta$ (i.e., if $\theta = \pi/4$). In this case $\cos \theta = 1/\sqrt{2}$ and from eq. (D4) we obtain $a = 1/2$, which corresponds to the CV whose gradient is $(\mathbf{e}_x + \mathbf{e}_y)/2$. The physically acceptable solutions given by eq. (D5) are a_+ when $\theta \in [0, \pi/4[$ and a_- when $\theta \in]\pi/4, \pi/2]$

2. Determination of the “Trial” Separatrix

Corresponding to the chosen CV (i.e., to θ) is the “trial” separatrix $\mathcal{S}(\theta)$, which is a line having the equation

$$y = m(x - x_{\max}), \quad (\text{D6})$$

where the point $(x_{\max}, 0)$ is the TS. The slope m is determined by requiring $\nabla \xi$ to be orthogonal to the unit vector parallel with $\mathcal{S}(\theta)$, which is given by

$$\mathbf{e}_{\mathcal{S}(\theta)} = \frac{-\mathbf{e}_x + m\mathbf{e}_y}{\sqrt{1 + m^2}}. \quad (\text{D7})$$

The orthogonality condition

$$\nabla \xi \cdot \mathbf{e}_{\mathcal{S}(\theta)} = (a\mathbf{e}_x + (1 - a)\mathbf{e}_y) \cdot \frac{-\mathbf{e}_x + m\mathbf{e}_y}{\sqrt{1 + m^2}} = 0 \quad (\text{D8})$$

yields $m = a/(1-a)$, which, when substituted back into eq. (D7), gives

$$\mathbf{e}_{S(\theta)} = \frac{(a-1)\mathbf{e}_x + a\mathbf{e}_y}{\sqrt{a^2 + (1-a)^2}}. \quad (\text{D9})$$

3. Computation of the Probability Density

The marginal probability density is given by

$$\rho(z) = Z^{-1} \int dx \int dy e^{-\beta U(x,y)} \delta(\xi(x,y) - z) \quad (\text{D10})$$

where

$$Z = \int dx \int dy e^{-\beta U(x,y)}. \quad (\text{D11})$$

To facilitate the evaluation of the double integrals, we transform from Cartesian coordinates to the orthogonal coordinates defined by

$$q_1 = \xi(x,y) = ax + (1-a)y \quad (\text{D12})$$

$$q_2 = (a-1)x + ay. \quad (\text{D13})$$

That $\nabla q_1 \cdot \nabla q_2 = 0$ is manifest. The inverse transformation is

$$\begin{aligned} x &= \frac{aq_1 + (a-1)q_2}{d} \\ y &= \frac{(1-a)q_1 + aq_2}{d}, \end{aligned} \quad (\text{D14})$$

where $d = a^2 + (1-a)^2$. Hence, the Jacobian is

$$\begin{aligned} \mathbf{J} &= \begin{pmatrix} \partial x / \partial q_1 & \partial x / \partial q_2 \\ \partial y / \partial q_1 & \partial y / \partial q_2 \end{pmatrix} \\ &= \begin{pmatrix} a/d & (a-1)/d \\ (1-a)/d & a/d \end{pmatrix} \end{aligned} \quad (\text{D15})$$

From eq. (D10) we have

$$\begin{aligned} \rho(z) &= Z^{-1} \int dq_1 \int dq_2 |\mathbf{J}| e^{-\beta U(x,y)} \delta(q_1 - z) \\ &= Z^{-1} \int dq_2 |\mathbf{J}| e^{-\beta U(x,y)}, \end{aligned} \quad (\text{D16})$$

where the Cartesian coordinates that are the arguments of the PES are given in terms of $q_1 = \xi$ and q_2 by eq. (D14).

Using eq. (D15) and the definition of d , we get $|\mathbf{J}| = 1/d$. Hence,

$$\rho(z) = \frac{\int dq_2 e^{-\beta U(x,y)}}{\int dq_1 \int dq_2 e^{-\beta U(x,y)}} \quad (\text{D17})$$

Appendix E: Computation of the Frequency of Crossing the Dividing Surface

We describe here the numerical implementation of the expression for ν (eq. (A1)) in the MD simulation.

1. Details of the MD Simulation

For each simulation corresponding to a given temperature and particle mass, ten independent Langevin dynamics simulations were carried out with a friction constant of 1 ps^{-1} , a time step of 1 fs , and a total time of 10 ns . The system was propagated using the velocity Verlet algorithm. Crossing frequencies and activation free energies were computed for each simulation independently, only the final values were used for averages and estimation of the standard deviation.

2. Use of the Heaviside Function

Approximating the time derivative by the forward finite-difference formula, we rewrite eq. (A1) as

$$\begin{aligned} \nu &= \frac{1}{\tau} \sum_{i=1}^{N_f-1} \Delta t \left| \frac{\Theta(\xi(t_{i+1}) - z_{\text{TS}}) - \Theta(\xi(t_i) - z_{\text{TS}})}{\Delta t} \right| \\ &= \frac{1}{\tau} \sum_{i=1}^{N_f-1} |\Theta(\xi(t_{i+1}) - z_{\text{TS}}) - \Theta(\xi(t_i) - z_{\text{TS}})|, \end{aligned} \quad (\text{E1})$$

where the summation on i is over consecutive time steps of length Δt , N_f is the number of steps of the MD simulation, and $\tau = (N_f - 1)\Delta t$ is the duration of the MD trajectory. That the expression in eq. (E1), which is straightforward to implement, yields a proper count may be seen as follows. If, at time step i , $\xi(t_i)$ and $\xi(t_{i-1})$ are both greater than or less than z_{TS} , the contribution is zero, since z_{TS} is not crossed during the step. If, on the other hand, $\xi(t_{i-1}) < z_{\text{TS}}$ and $\xi(t_i) > z_{\text{TS}}$, or $\xi(t_{i-1}) > z_{\text{TS}}$ and $\xi(t_i) < z_{\text{TS}}$, then the contribution is 1, as z_{TS} is crossed in one direction or the other during the step. We note that Δt must be sufficiently small that highly frequent crossings are not inadvertently missed.

3. Use of the Dirac Delta Function and the Atomic Velocities

We consider here an alternative approach to the computation of ν . We begin by recasting eq. (A2) as

$$\nu = \lim_{\tau \rightarrow \infty} \frac{1}{\tau} \int_0^\tau dt \delta[\xi(t) - z_{\text{TS}}] |(\nabla_x \xi)^T \cdot \dot{\mathbf{x}}(t)|. \quad (\text{E2})$$

Here we express the rate of change of the CV as

$$\dot{\xi}(t) = \frac{d\xi}{dt} \cdot \frac{d\mathbf{x}}{dt} = (\nabla_x \xi)^T \cdot \dot{\mathbf{x}}(t), \quad (\text{E3})$$

where $(\nabla_x \xi)^T = (\partial \xi / \partial x_1, \partial \xi / \partial x_2, \dots, \partial \xi / \partial x_{3N})$ is the 3N-dimensional gradient. Discretizing the integration on

time, we rewrite eq. (E2) as

$$\begin{aligned}\nu &= \frac{1}{\tau} \sum_{i=0}^{N_f-1} \Delta t \delta[\xi(t_i) - z_{\text{TS}}] |(\nabla_x \xi(t_i))^T \cdot \dot{\mathbf{x}}(t_i)| \\ &= \frac{1}{N_f - 1} \sum_{i=0}^{N_f-1} \delta[\xi(t_i) - z_{\text{TS}}] |(\nabla_x \xi(t_i))^T \cdot \dot{\mathbf{x}}(t_i)| .\end{aligned}\quad (\text{E4})$$

In practice, of course, the duration of the MD simulation, and therefore the number of time steps, are finite. It is very unlikely that during a finite simulation $\xi(t_i)$ is ever exactly equal to z_{TS} . Hence, almost every configuration $\mathbf{x}(t)$ gives zero contribution. To circumvent this problem we introduce a continuous function to represent the delta function approximately. We begin by defining the continuous approximation to the Heaviside function

$$\Theta(x; \alpha) = \frac{1}{1 + e^{-\alpha x}} , \quad (\text{E5})$$

where α is a positive real number having dimension reciprocal length. (Observe that we can formally express the true Heaviside “function” by $\Theta(x) = \lim_{\alpha \rightarrow \infty} \Theta(x; \alpha)$.) The corresponding delta function is given by the derivative

$$\delta(x; \alpha) = \frac{d\Theta(x; \alpha)}{dx} = \frac{\alpha e^{-\alpha x}}{(1 + e^{-\alpha x})^2} . \quad (\text{E6})$$

Note that $\delta(x; \alpha)$ satisfies exactly the relation

$$\int_{-\infty}^{\infty} dx \delta(x; \alpha) = 1 . \quad (\text{E7})$$

We can now rewrite eq. (E4) as

$$\nu_\alpha = \frac{1}{N_f - 1} \sum_{i=0}^{N_f-1} \delta[\xi(t_i) - z_{\text{TS}}; \alpha] |(\nabla_x \xi(t_i))^T \cdot \dot{\mathbf{x}}(t_i)| , \quad (\text{E8})$$

where $\delta[\xi(t_i) - z_{\text{TS}}; \alpha]$ is approximated by eq. (E6). The index α emphasizes the dependence of the crossing frequency on this methodological parameter.

The quality of this approximation depends on the choice of α . On one hand, if α is too small, MD frames that are far away from the dividing surface contribute significantly, thus yielding too large ν . On the other hand, if α is too large, all frames are weighted so lightly that ν is too small. The influence of α is shown graphically in Fig. 10. Note that we plot the magnitude of the difference so that small differences are visible on the logarithmic scale. One can clearly see that extreme choices of α can lead to errors in ν of up to a factor of 100. As predicted, ν_α tends to zero for very large α ,

which is reflected by the curves approaching 1 (10^0). The optimal choice of α seems to be between 10^2 and 10^3 . Even choices in the range 10^1 to 10^4 generally yield ν_α ’s which are around $0.9\nu_{\text{ref}}$ to $1.1\nu_{\text{ref}}$, which corresponds at 300 K to an error of approximately 0.25 kJ/mol in $\Delta F_{\text{RP}}^\ddagger$.

Appendix F: Plots of the FEPs for Models of Section V A with Large ϵ

In Section V A of the article we consider two CVs: $\xi_1(x) = x$ and $\xi_2(x) = 1/(x + 5)$. Fig. 11a shows the the PES eq. (46) for the case $a = 1 \text{ \AA}^{-2}$, $b = 1 \text{ \AA}$, and $\epsilon = 50 \text{ kJ/mol}$. Figs. 11b and 11c show plots of the FEPs based on the two CVs just as does Fig. 5 of the article.

Appendix G: Computation of FEPs for the Cyclization of the Hexenyl Radical

Ab-initio MD simulations on DFT level were performed using a development version of the FermiONs++ program package^{69–72}. For this purpose the $\omega\text{B97M-V}$ functional was applied with the def2-TZVP basis set^{49,73}. To account for solvation in benzene the COSMO continuum solvation model was used⁵⁰. An optimized minimum energy structure was heated from 0.1 K to 310 K over 3100 time steps with a step size of 0.1 fs. Initial momenta were randomly drawn from the Maxwell-Boltzmann distribution. Velocities were re-scaled every 10 time steps to increase the temperature by 1 K. For production runs the temperature was controlled by a Langevin thermostat with friction coefficient 0.001 fs^{-1} at 300 K. The time step was set to 0.5 fs. The dynamics was biased along reaction coordinates $\xi = d(\text{C1} - \text{C5})$ with the WTM-eABF method^{52,53} applying a recently published Python implementation⁵⁴. For simulations along ξ the extended-variable was coupled to the reaction coordinate with a thermal width of 0.05 \AA and the system was confined with harmonic walls at 1.0 \AA and 6.0 \AA . The bias force was stored on a grid with bin width 0.05 \AA . The ABF force was scaled up linearly and the full bias applied in bins with more than 200 samples. For the Well-Tempered Metadynamics (WTM) potential Gaussian kernels of height 0.5 kJ/mol and standard deviation 0.1 \AA for ξ were deposited every 20 steps. The height of new Gaussian hills was scaled down over the course of the simulation with effective temperature of 2000 K. Sampling of ξ was performed with a single walker running for about 290 ps.

To obtain thermodynamic properties statistical weights of individual frames were recovered in post-processing using the MBAR algorithm⁴⁵. For this purpose the sampled probability distribution was re-partitioned into a mixture of Gaussian distributions with standard deviation 0.05 \AA for ξ ⁵⁴.

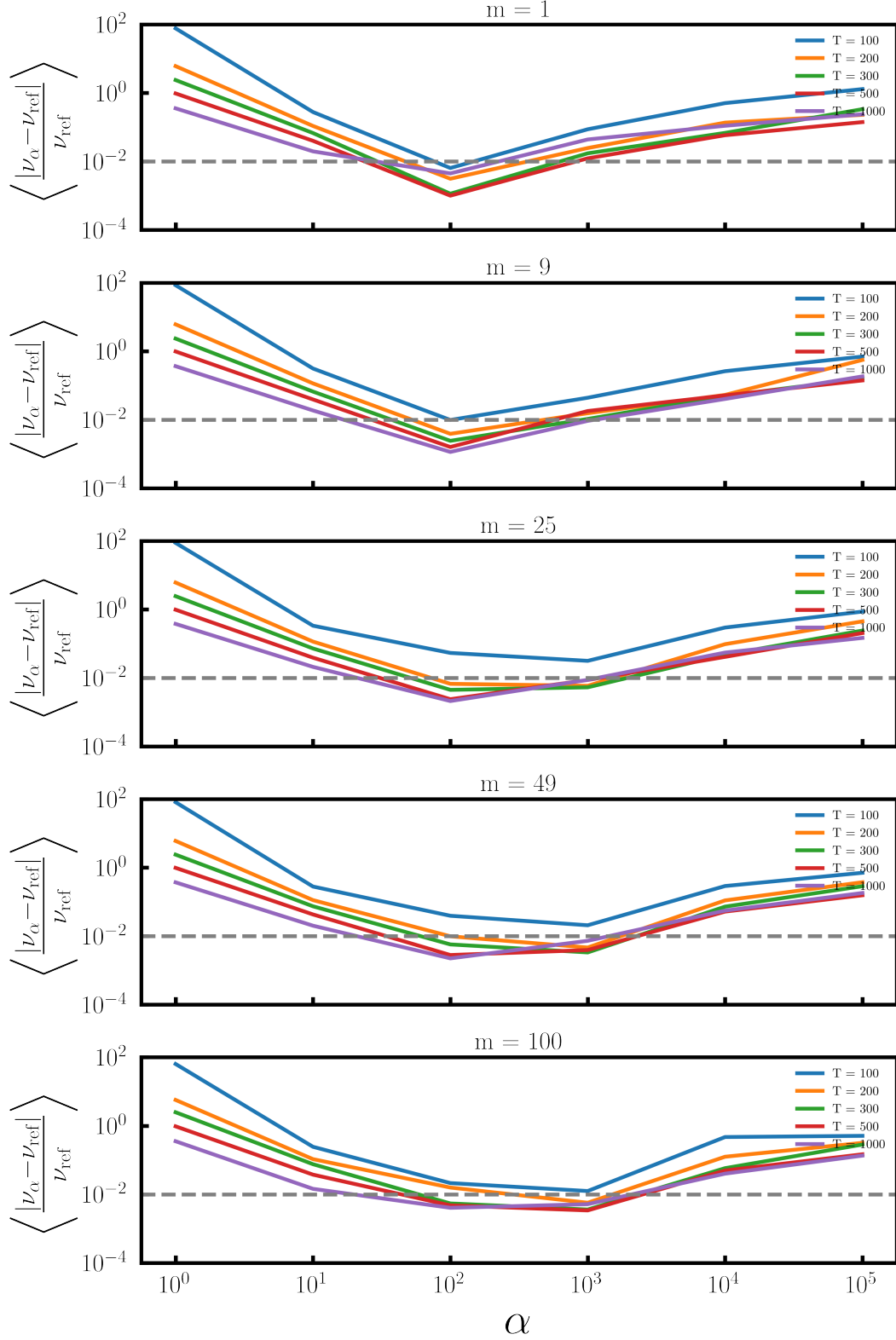


FIG. 10. Plots of the magnitude of relative difference between reference crossing frequency computed by eq. (S35) and that computed by eq. (S40) versus α for the one-dimensional model PES in Section V A ($\epsilon = 5$ kJ/mol) for a selection of masses and temperatures. Each curve is an average over 10 independent MD trajectories. The grey dashed line marks the threshold of 1 % relative deviation.

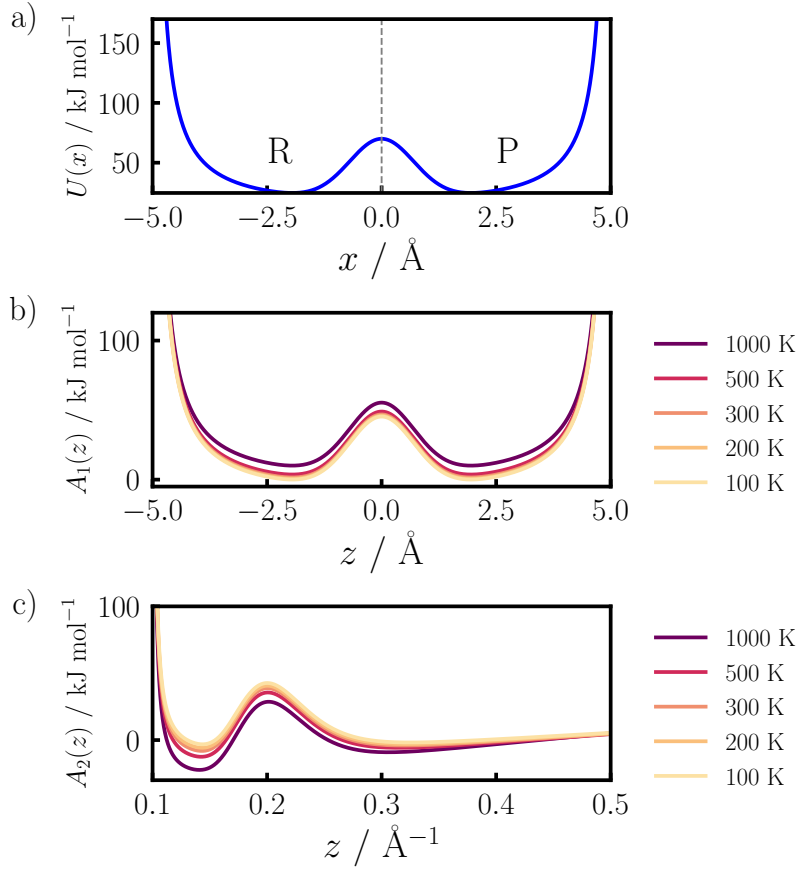


FIG. 11. a) PES $U(x)$ with $\epsilon = 50 \text{ kJ/mol}$ (eq. (46)); b) FEP for CV $\xi = x$; c) FEP for CV $\xi = \frac{1}{x+5}$.